# CHARACTERISTICS, TIMING, AND HAZARD POTENTIAL OF LIQUEFACTION-INDUCED LANDSLIDING IN THE FARMINGTON SIDING LANDSLIDE COMPLEX, DAVIS COUNTY, UTAH

*by*

*Michael D. Hylland and Mike Lowe*

*Trench exposure of liquefied sand and disrupted silt interbed.*

*Backhoe trench excavated on a hummock sideslope within the Farmington Siding landslide complex, with the Wasatch Range in the background.*

*Block of organic soil incorporated into landslide deposits during landsliding.*

**SPECIAL STUDY 95 1998**
**UTAH GEOLOGICAL SURVEY**
*a division of*
Utah Department of Natural Resources

## STATE OF UTAH

*Michael O. Leavitt, Governor*

## DEPARTMENT OF NATURAL RESOURCES

*Ted Stewart, Executive Director*

## UTAH GEOLOGICAL SURVEY

*M. Lee Allison, Director*

### UGS Board

| Member | Representing |
|---|---|
| Russell C. Babcock, Jr. (Chairman) | Mineral Industry |
| D. Cary Smith | Mineral Industry |
| Craig Nelson | Civil Engineering |
| E.H. Deedee O'Brien | Public-at-Large |
| C. William Berge | Mineral Industry |
| Jerry Golden | Mineral Industry |
| Richard R. Kennedy | Economics-Business/Scientific |
| David Terry, Director, Trust Lands Administration | *Ex officio member* |


## UTAH GEOLOGICAL SURVEY

The **UTAH GEOLOGICAL SURVEY** is organized into five geologic programs with Administration, Editorial, and Computer Resources providing necessary support to the programs. The **ECONOMIC GEOLOGY PROGRAM** undertakes studies to identify coal, geothermal, uranium, hydrocarbon, and industrial and metallic resources; initiates detailed studies of these resources including mining district and field studies; develops computerized resource data bases, to answer state, federal, and industry requests for information; and encourages the prudent development of Utah's geologic resources. The **APPLIED GEOLOGY PROGRAM** responds to requests from local and state governmental entities for engineering-geologic investigations; and identifies, documents, and interprets Utah's geologic hazards. The **GEOLOGIC MAPPING PROGRAM** maps the bedrock and surficial geology of the state at a regional scale by county and at a more detailed scale by quadrangle. The **GEOLOGIC EXTENSION SERVICE** answers inquiries from the public and provides information about Utah's geology in a non-technical format. The **ENVIRONMENTAL SCIENCES PROGRAM** maintains and publishes records of Utah's fossil resources, provides paleontological and archeological recovery services to state and local governments, conducts studies of environmental change to aid resource management, and evaluates the quantity and quality of Utah's ground-water resources.

The UGS Library is open to the public and contains many reference works on Utah geology and many unpublished documents on aspects of Utah geology by UGS staff and others. The UGS has several computer data bases with information on mineral and energy resources, geologic hazards, stratigraphic sections, and bibliographic references. Most files may be viewed by using the UGS Library. The UGS also manages a sample library which contains core, cuttings, and soil samples from mineral and petroleum drill holes and engineering geology investigations. Samples may be viewed at the Sample Library or requested as a loan for outside study.

The UGS publishes the results of its investigations in the form of maps, reports, and compilations of data that are accessible to the public. For information on UGS publications, contact the Natural Resources Map/Bookstore, 1594 W. North Temple, Salt Lake City, Utah 84116, (801) 537-3320. E-mail: nrugs.geostore@state.ut.us and visit our web site at http://utstdpwww.state.ut.us/~ugs/bookstor.htm.


### UGS Editorial Staff

| | |
|---|---|
| J. Stringfellow | Editor |
| Vicky Clarke, Sharon Hamre | Graphic Artists |
| Patricia H. Speranza, James W. Parker, Lori Douglas | Cartographers |



*The Utah Department of Natural Resources receives federal aid and prohibits discrimination on the basis of race, color, sex, age, national origin, or disability. For information or complaints regarding discrimination, contact Executive Director, Utah Department of Natural Resources, 1594 West North Temple #3710, Box 145610, Salt Lake City, UT 84116-5610 or Equal Employment Opportunity Commission, 1801 L Street, NW, Washington DC 20507.*

TAKE Pride IN UTAH

Printed on recycled paper


2/98

# CHARACTERISTICS, TIMING, AND HAZARD POTENTIAL OF LIQUEFACTION-INDUCED LANDSLIDING IN THE FARMINGTON SIDING LANDSLIDE COMPLEX, DAVIS COUNTY, UTAH

*by*

*Michael D. Hylland and Mike Lowe*

Research supported by the U.S. Geological Survey (USGS), Department of the Interior, under USGS award number 1434-94-G-2498. The views and conclusions contained in this document are those of the authors and should not be interpreted as necessarily representing the official policies, either expressed or implied, of the U.S. Government.

**SPECIAL STUDY 95 1998**
**UTAH GEOLOGICAL SURVEY**
*a division of*
**Utah Department of Natural Resources**

# CONTENTS



# ILLUSTRATIONS

## TABLES

# CHARACTERISTICS, TIMING, AND HAZARD POTENTIAL OF LIQUEFACTION-INDUCED LANDSLIDING IN THE FARMINGTON SIDING LANDSLIDE COMPLEX, DAVIS COUNTY, UTAH

*by*
*Michael D. Hylland and Mike Lowe*

## ABSTRACT

The Farmington Siding landslide complex covers approximately 19.5 square kilometers (7.5 mi2) in Davis County, Utah. The landslide complex consists of liquefaction-induced landslides that show evidence of recurrent movement during latest Pleistocene and Holocene time. This study qualitatively assesses the hazard associated with future liquefaction-induced landsliding by evaluating slope-failure modes and extent of internal deformation within the landslide complex, inferring the geologic and hydrologic conditions under which landsliding occurred, determining the timing of landsliding, and evaluating the relative likelihood of various earthquake source zones to trigger liquefaction-induced landsliding at the Farmington Siding landslide complex.

The landslide deposits comprise fine-grained, late Pleistocene to Holocene lacustrine sediments of Lake Bonneville and Great Salt Lake. Geotechnical borehole data confirm the presence of liquefiable sand and silt in the shallow subsurface within the landslide complex, and geologic evidence for liquefaction includes injected sand, attenuation and disruption of silt and clay interbeds within sand beds, and failure of very gentle slopes not otherwise susceptible to landsliding. Both lateral spread and flow have been important slope-failure modes, but flow has had a dominant influence on the morphology of the complex.

Relative and absolute timing information indicates at least three, and possibly four, landslide events: the first sometime between 14,500 and 10,900 $^{14}$C yr B.P.; the second just prior to 7,310 ± 60 $^{14}$C yr B.P. (8,100 [+250, -200] cal yr B.P.); the third(?) sometime prior to 5,280 ± 60 $^{14}$C yr B.P. (6,000 [+300, -250] cal yr B.P.); and the fourth between 2,340 ± 60 and 2,440 ± 70 $^{14}$C yr B.P. (2,750 and 2,150 cal yr B.P.). The landslide events generally progressed from south to north, and the southern part of the complex has remained relatively stable during the late Holocene. The timing of these landslide events corresponds well with the timing of Great Salt Lake highstands and associated high ground-water levels, as well as with the timing of documented large earthquakes on the Wasatch fault zone. Thus, relatively major landsliding is likely associated with large earthquakes coincident with high lake and ground-water levels.

Numerous earthquake source zones have been active in northern Utah during the Holocene. Empirical earthquake magnitude-distance relations indicate that liquefaction-induced landsliding at the Farmington Siding landslide complex could have been triggered by large earthquakes on the East Cache, East Great Salt Lake, West Valley, and Oquirrh fault zones, as well as the Brigham City, Weber, Salt Lake City, Provo, and possibly Nephi segments of the Wasatch fault zone. However, comparison of expected peak horizontal ground accelerations with calculated critical accelerations, as well as quantitative estimates of liquefaction severity index and Newmark landslide displacements, point to large earthquakes on the nearby Weber segment as being the most likely to trigger significant liquefaction-induced landsliding at the Farmington Siding landslide complex.

The susceptibility to liquefaction-induced landsliding in the vicinity of the Farmington Siding landslide complex may presently be less than at other times during the Holocene, given the lower average lake and associated ground-water levels during historical time as compared to those that characterized much of the Holocene. However, a higher potential for liquefaction-induced landsliding would exist if the area experienced strong ground shaking during a time of increased soil pore-water pressures associated with abnormally high lake and/or ground-water levels. Based on geologic conditions and the pattern of previous landsliding, the relative hazard associated with liquefaction-induced landsliding is higher in the northern part of the landslide complex and in the crown area adjacent to the north and northeast margins of the complex, and is lower in the southern part of the landslide complex and in the flank and crown areas adjacent to the northwest, east, and southeast margins of the complex. Given the rel-

ative likelihood of a large earthquake in this part of Utah in the near future and the possible consequences of large-displacement slope failure involving lateral spread or flow, special consideration of the potential for liquefaction-induced landsliding in the northern part of the complex and in the crown area north and northeast of the complex is warranted in land-use planning.

## INTRODUCTION

The Farmington Siding landslide complex is in Davis County, Utah, about 25 kilometers (15 mi) north of Salt Lake City (figure 1). The landslide complex covers approximately 19.5 square kilometers (7.5 mi$^2$) and is one of 13 late Pleistocene/Holocene features along the Wasatch Front mapped by previous investigators as possible liquefaction-induced lateral spreads. The Farmington Siding landslide complex is in a largely rural area, but state and interstate highways, railroads, petroleum and natural-gas pipelines, and other lifelines cross the complex. Continued population growth along the Wasatch Front increases the likelihood of urban development within and adjacent to the landslide complex. Development along the Wasatch Front has proceeded with little consideration of hazards associated with liquefaction-induced landslides. Slope-failure mechanisms, extent of internal deformation, and timing of landslide events are poorly understood, and these factors must be evaluated to enable local governments to effectively plan for development and implement hazard-reduction strategies as needed.

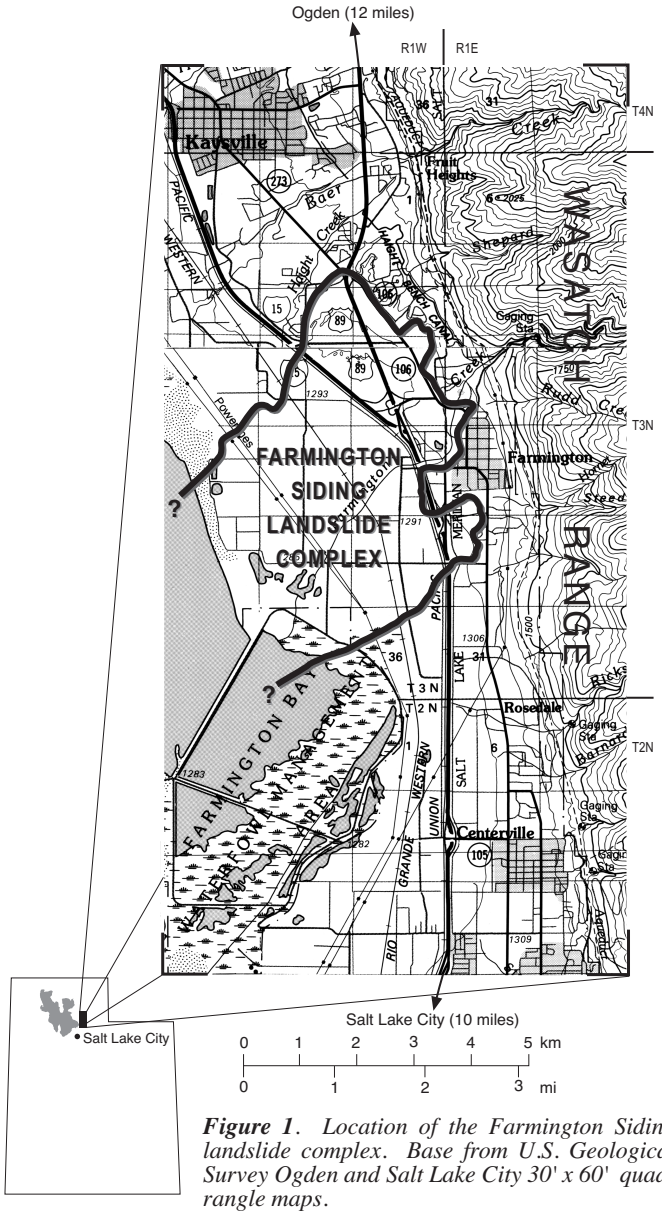


***Figure 1**. Location of the Farmington Siding landslide complex. Base from U.S. Geological Survey Ogden and Salt Lake City 30' x 60' quadrangle maps.*

The purpose of this study is to assess the hazard associated with future liquefaction-induced landsliding within and adjacent to the Farmington Siding landslide complex by evaluating slope-failure modes and extent of internal deformation within the complex, inferring the geologic and hydrologic conditions under which landsliding occurred, determining the timing of landsliding, and evaluating the relative likelihood of various earthquake source zones to trigger liquefaction-induced landsliding. We chose the Farmington Siding landslide complex for this study because of the distinctiveness of geomorphic features on the northern part of the complex and the presence of landslide deposits that are clearly of different ages. Furthermore, because much of the area is rural, appropriate land-use planning measures can still be implemented to protect future development.

This study was sponsored jointly by the Utah Geological Survey and U.S. Geological Survey, with partial funding provided through the National Earthquake Hazards Reduction Program (NEHRP). Results of the study were originally presented in a final technical report to the U.S. Geological Survey (Hylland and Lowe, 1995).

## PREVIOUS WORK

The Farmington Siding landslide complex was first identified by Van Horn (1975). He recognized two ages of landsliding in the complex, based in part on differences in soil development on the landslide deposits. He also noted that the younger (northern) landslide disrupts the Gilbert shoreline of Great Salt Lake, but was unable to determine the relation between the older (southern) landslide and the Gilbert shoreline. Van Horn (1975) assigned an age of 2,000 years or less to the younger landslide and 2,000 to 5,000 years to the older landslide based on soil development and his assumed age of the Gilbert shoreline. The landslide complex and adjacent areas were later mapped by Miller (1980), Anderson and others (1982), and Nelson and Personius (1993). Miller (1980) and Anderson and others (1982) mapped two landslides of different ages in the complex after Van Horn (1975). Both of these maps indicate the younger landslide truncates the Gilbert shoreline. The maps differ, however, in that Anderson and others (1982) mapped the Gilbert shoreline across and ad-

jacent to the southern margin of the older landslide, whereas Miller (1980) did not. Nelson and Personius (1993) mapped the complex as three separate landslides and note (p. 13) that the younger, northern landslide "...clearly postdates the Gilbert shoreline...," but they did not map the Gilbert shoreline across either of the two older landslides in the southern part of the complex.

Anderson and others (1982) summarize the results of subsurface geotechnical investigations for numerous sites within the Farmington Siding landslide complex. Additionally, Miller and others (1981) drilled two test holes within the landslide complex, and Chen and Associates (1988) investigated a site near the middle of the complex for the Davis County Criminal Justice Complex. The toe area of the northern part of the landslide complex may have been encountered during a drilling project in Farmington Bay to test foundation conditions for a proposed water-storage reservoir (Everitt, 1991). Inclined and deformed bedding in lacustrine sediments, attributed to landsliding, was encountered in drill holes to a maximum of about 21 meters (70 ft) below the bottom of the bay. An organic clay layer immediately overlying the landslide deposit yielded a radiocarbon age of 2,930 ± 70 $^{14}$C yr B.P. (Everitt, 1991).

Detailed mapping and limited trenching of the Farmington Siding landslide complex were completed as part of a study of possible liquefaction-induced landslides along the Wasatch Front (Harty and others, 1993; Lowe and others, 1995). Harty and others (1993) concluded that both lateral spread and flow have occurred within the landslide complex. They mapped two landslides of different ages within the complex, and recognized the Gilbert shoreline as preserved across the southern landslide. Calendar-calibrated radiocarbon age estimates for soils obtained by Harty and others (1993) from the northern landslide indicate movement sometime after 4,530 ± 300 cal yr B.P. but before 2,730 ± 370 cal yr B.P. Harty and others (1993) believe the northern landslide formed closer to the younger date, possibly during either the penultimate or antepenultimate surface-faulting earthquake on the nearby Weber segment of the Wasatch fault zone.

## GEOLOGY AND GEOMORPHOLOGY

The Farmington Siding landslide complex is in a gently sloping area underlain primarily by fine-grained, stratified, late Pleistocene to Holocene lacustrine deposits of Lake Bonneville and Great Salt Lake (Van Horn, 1975; Miller, 1980; Anderson and others, 1982; Harty and others, 1993; Lowe and Harty, 1993; Nelson and Personius, 1993; Lowe and others, 1995) (figures 2 and 3). The crown is underlain primarily by Lake Bonneville sand and silt deposits and is at an elevation of about 1,340 meters (4,400 ft) in the vicinity of the city of Farmington. Holocene marsh deposits are present in topographically low areas, especially near Farmington Bay at an elevation of about 1,281 meters (4,200 ft). Post-Lake Bonneville

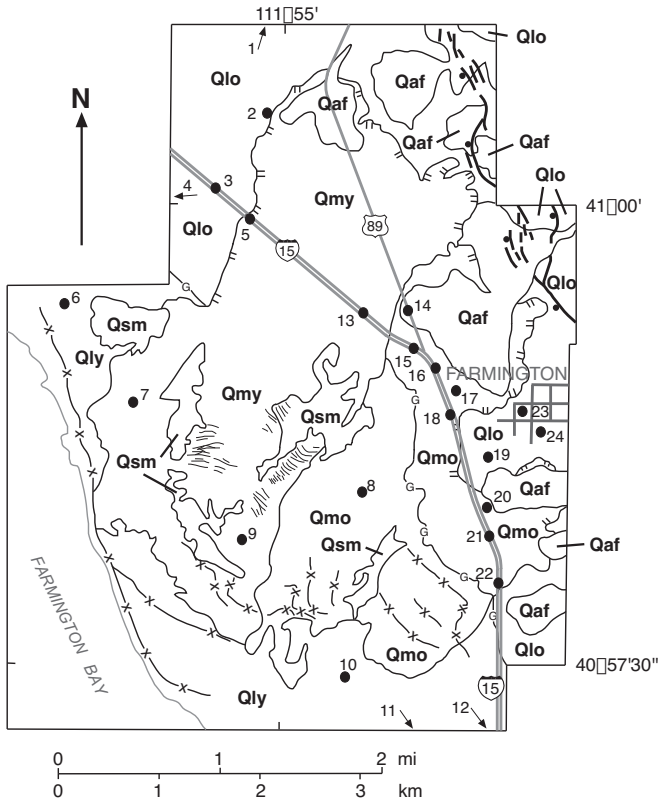


**EXPLANATION**

**Map Units**

| | |
|---|---|
| Qmy | Younger mass-movement (lateral spread and flow) deposits |
| Qmo | Older mass-movement (lateral spread and flow) deposits |
| Qaf | Alluvial-fan and debris-flow deposits |
| Qsm | Marsh deposits |
| Qly | Younger lacustrine (Great Salt Lake) deposits |
| Qlo | Older lacustrine (Lake Bonneville) deposits |

**Map Symbols**

Landslide scarp

Normal fault; ball on downthrown side

Lineament

Gilbert shoreline

Other shorelines of Great Salt Lake

Geotechnical borehole site from Anderson and others (1982); arrow indicates site off map

***Figure 2.*** *Simplified geologic map of the Farmington Siding landslide complex (modified from Harty and others, 1993), and borehole sites from which geotechnical data summarized in table 1 were obtained.*

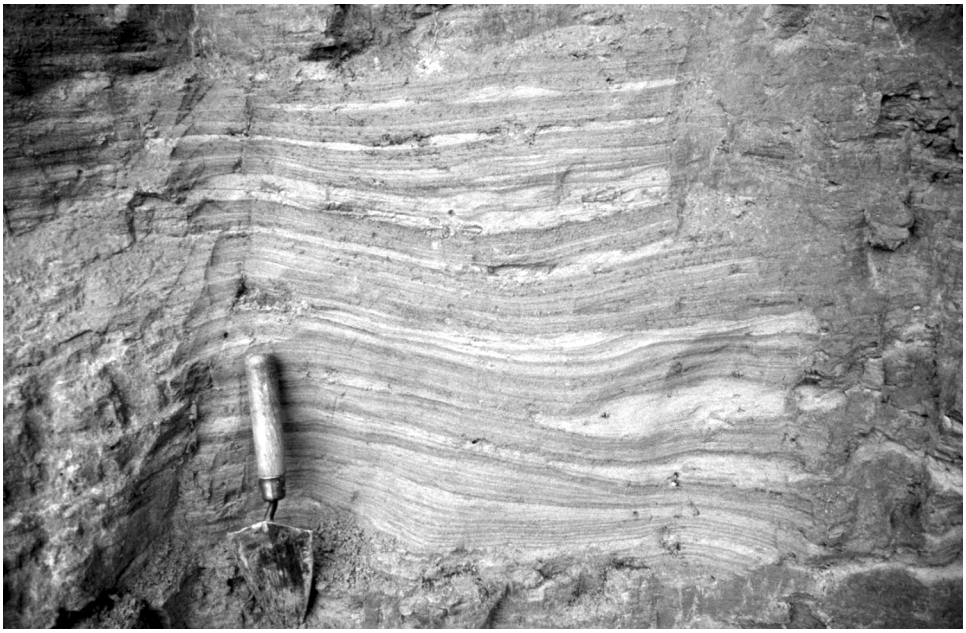

***Figure 3***. *Pleistocene lacustrine deposits of Lake Bonneville consisting of thin-bedded sand and silt, exposed in a road cut along Swinton Lane in the landslide main scarp (see figure 5 for location). Trowel for scale.*

alluvial-fan and debris-flow deposits overlie the lacustrine deposits in places along the eastern and northern margins of the landslide complex. Streams flowing westward from the Wasatch Range have locally dissected the landslide main scarp, which is clearly visible along the northwest to northeast margin of the complex.

Ground slopes within the landslide complex range from about 0.4 to 0.8 percent (0.3-0.5 degree). Unfailed slopes adjacent to the complex range from about 1 to 2 percent (0.6-1 degree) along the flanks and 6 to 11 percent (3-6 degrees) in the crown areas east of the complex. The head region in the northern and eastern parts of the landslide complex generally displays negative topographic relief (zone of depletion), whereas the distal region in the western part of the complex generally displays slight positive topographic relief (zone of accumulation).

Landslide geomorphology includes scarps, hummocks, closed depressions, and transverse lineaments. Well-preserved lateral and main scarps in the northern part of the complex range in height from about 3 to 12 meters (10-40 ft). Hummocks and closed depressions are present over most of the complex, but are more common in the northern part (Harty and others, 1993) (figure 4). Hummocks on the northern part are morphologically distinct, having as much as about 6 meters (20 ft) of relief and lateral dimensions ranging from tens to hundreds of meters. Hummocks on the southern part of the complex are morphologically subtle, generally having less than about 2 meters (6 ft) of relief. The hummocks are typically elongate and parallel to the main scarp in the northwestern part of the complex, but become more randomly oriented with increasing distance from the head (Van Horn, 1975; Harty and others, 1993). Subtle transverse lineaments are present in the central part of the complex (Harty and others, 1993).

## TRENCH DESCRIPTIONS

As a follow-up to the mapping and trenching of Harty and others (1993), we excavated five backhoe trenches within the Farmington Siding landslide complex between December 1994 and March 1995 to further evaluate slope-failure mode and extent of internal deformation, and to obtain datable soil samples to refine landslide-timing estimates. Existing development and land use, property ownership, and shallow ground water placed limitations on trench locations. Four trenches (FST1, FST2, FST3, and FST4) were within the northern (younger) landslide of Harty and others (1993), and one (FST5) was across the boundary between their younger and older landslides (figure 5). We logged geologic and soil units on a planimetric base constructed on a 1-meter by 1-meter grid using level lines. Refer to appendix A for detailed unit descriptions. Soil-


***Figure 4***. *Aerial view toward the northwest showng hummocky landslide terrain on northern part of Farmington Siding landslide complex. Approximate position of landslide main scarp indicated by dashed line with hachures. Hummocks appear as irregularly shaped lighter areas.*

horizon nomenclature follows the U.S. Soil Conservation Service description system (Soil Survey Staff, 1981; Guthrie and Witty, 1982), and pedogenic carbonate horizons were classified using the system developed by Gile and others (1966) and Machette (1985) and modified by Birkeland and others (1991). Radiocarbon ages of organic soils encountered in the trenches, and implications for landslide-timing estimates, are discussed below under "Landslide Timing."

## Trench FST1

We excavated trench FST1 on the Oakridge Country Club golf course in the NE¼ section 14, T. 3 N., R. 1 W., Salt Lake Base Line and Meridian (SLBM) (figure 5), on the sideslope of a hummock interpreted to be a landslide block (figure 6). The trench was approximately 15.5 meters (51 ft) long and averaged 2 meters (7 ft) deep (figure 7). The trench exposed landslide deposits derived from

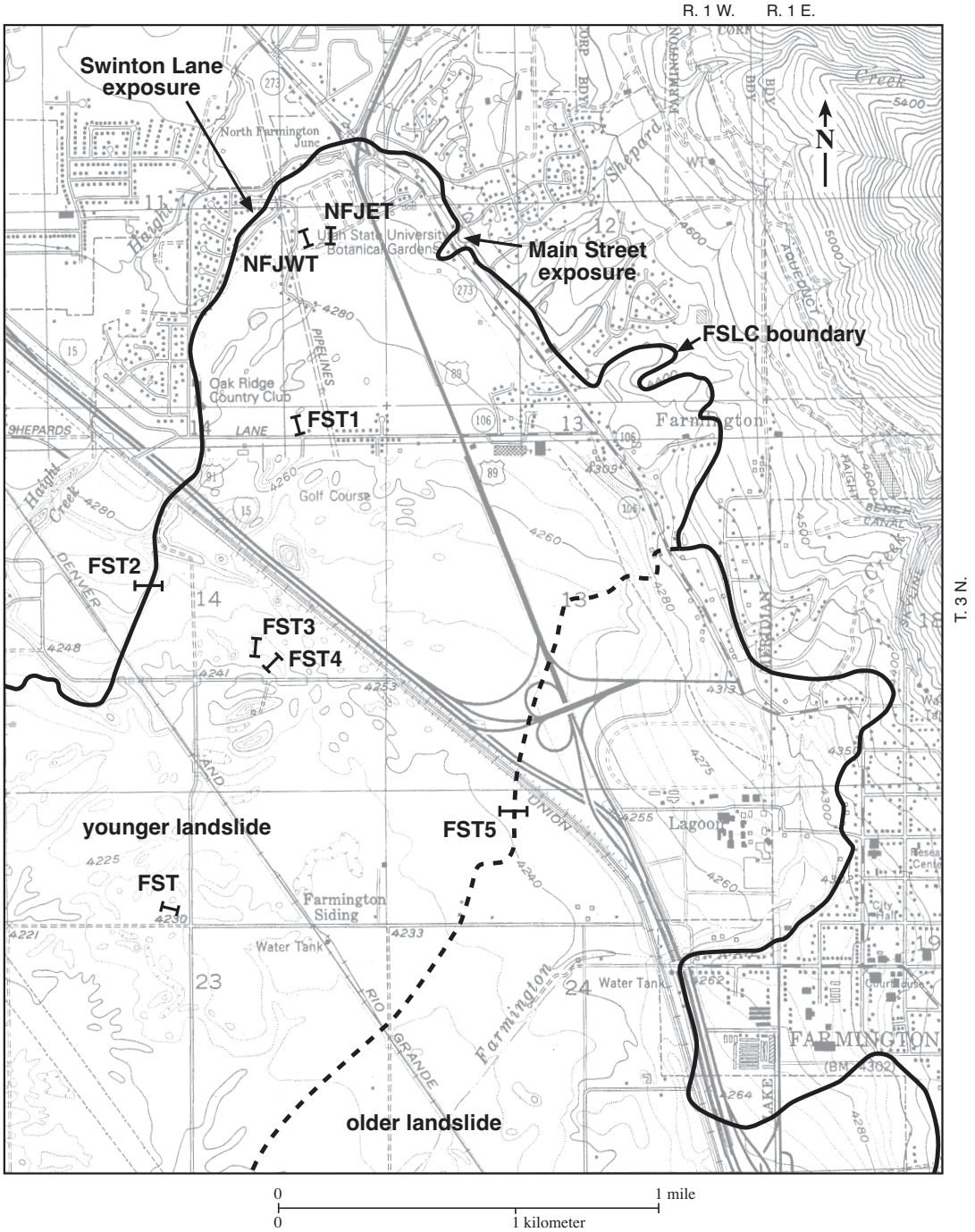


***Figure 5***. *Locations of trenches excavated on the Farmington Siding landslide complex during this study (FST1 through FST5), trenches excavated by Harty and others (1993) (NFJET, NFJWT, and FST), and Swinton Lane and Main Street exposures discussed in text. Boundary of landslide complex (solid line) and margin between younger and older landslides (dashed line) from Harty and others (1993). Note topographic expression of hummocks and depressions on younger landslide. Base from U.S. Geological Survey Farmington and Kaysville 7.5' quadrangle maps.*

lacustrine sediments (units 1, 2, and 3) consisting of interbedded well-sorted fine sand and clayey silt. The strata are generally inclined and/or gently folded with apparent dips as steep as 34 degrees, presumably due at least in part to backtilting of the block during landsliding. The strata have been disrupted along several discrete low- and high-angle faults. Although we observed no identifiable marker beds, the lack of matching strata across the dominant low-angle fault indicates at least 3 meters (10 ft) of apparent displacement along this structure. The low-angle fault is offset by a high-angle fault with approximately 30 centimeters (1 ft) of apparent dip slip. Conformable contacts between silt and sand beds in unit 2 near this high-angle fault are also offset along small-displacement (less than 3 centimeters [1 in]) faults. A sand bed in unit 3 near the upslope end of the trench appeared to have a well-developed boudinage structure perhaps associated with liquefaction, although this could also be a loading-related depositional feature.

***Figure 6.*** *Trench FST1, excavated on a hummock sideslope. View is toward the northwest.*

Trench FST1

Mapped by M.D. Hylland, C.E. Bishop, and G.E. Christenson

December 1994

Planimetric base constructed on a 1 m x 1 m grid

Computer drafted by B.H. Mayes

**EXPLANATION**

**UNIT DESCRIPTIONS**[1,2]

Modern soil:

| | |
|---|---|
| S1(A) | A horizon |
| S1(Bk) | Bk horizon (stage I+) |

Landslide deposits derived from lacustrine sediment:

| | |
|---|---|
| 3 | Brown to yellowish-brown interbedded clayey silt and sand |
| 2 | Brown to yellowish-brown interbedded sand and clayey silt |
| 1 | Olive-brown to brown interbedded sand and clayey silt |

**SYMBOLS**

- A horizon
- Unstratified sand
- Laminae in clay and silt
- Soil-unit boundary
- Geologic contact, dashed where indistinct
- Intra-unit contact
- Fault, dashed where indistinct (arrows show relative movement)

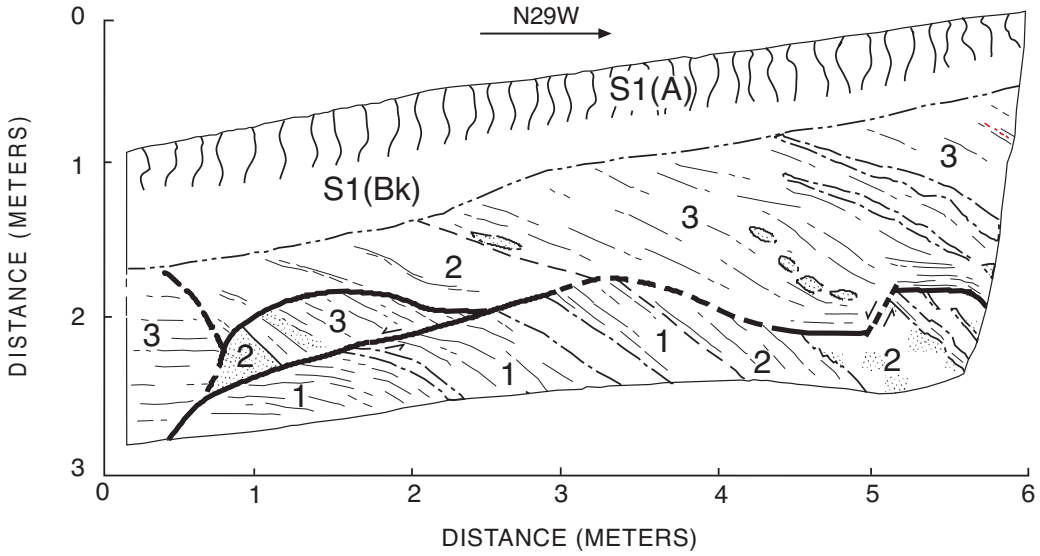


Footnotes:

1 See appendix A for detailed descriptions.

2 Units with same number on log are lithologically similar but not necessarily stratigraphically equivalent.

***Figure 7****. Log of trench FST1.*

A modern soil profile comprising A and Bk horizons is developed to a maximum depth of 80 centimeters (32 in) in FST1. The Bk horizon displayed stage I+ carbonate morphology.

## Trench FST2

We excavated trench FST2 in a hay field in the NW¼ section 14, T. 3 N., R. 1 W., SLBM (figure 5), on and approximately perpendicular to the trend of the landslide scarp (figure 8). The trench, which extended from the base of the scarp to approximately three-fourths of the way to the top of the scarp, was approximately 35 meters (115 ft) long and averaged 1.5 to 2 meters (5-7 ft) deep (figure 9). The base of the trench exposed lacustrine sediments consisting of unstratified, well-sorted fine sand with thin, disrupted silt interbeds (unit 1), overlain by laminated clayey silt (unit 2) locally cross-cut by sand dikes 1 to 4 centimeters (0.4-1.6 in) thick. The disruption of the silt interbeds and injection of the sand into the overlying clayey silt indicate liquefaction of unit 1. A Bk horizon consisting of units S1(Bk), S1(Bkb), and S2(Bk) comprises a paleosol on units 1 and 2. This Bk horizon displayed stage II carbonate morphology. Unit 2 and the Bk horizon have been offset at four locations by high-angle faults, presumably during landslide-scarp formation or modification. Offset of geologic and soil-unit boundaries at two of these faults indicated 85 centimeters (34 in) of cumulative vertical displacement. Vertical displacement could not be determined at the other two faults because of the lack of matching strata across the faults, but appeared to total at least 60 centimeters (24 in).

A wedge-shaped unit of probable colluvial origin (unit 3) overlies unit S1(Bkb). Unit 3 consists of unstratified, organic silty sand with clay and fine gravel, and displayed a pervasive pinhole (vesicular) soil texture. A weakly developed pedogenic carbonate morphology (stage I) is developed in this unit. Unit 3 is juxtaposed against units 2 and S1(Bk) along a sharp, high-angle contact interpreted to be a buried scarp free-face. Unit 3, therefore, apparently represents landslide-scarp-derived colluvium that was deposited on the surface of the downdropped landslide block shortly after scarp formation. No evidence for a buried A horizon underlying unit 3 was observed. However, the presence of a paleosol A horizon could be masked by accumulated secondary calcium carbonate, especially if the A horizon was thin and/or poorly developed.

A modern soil profile comprising A and Bk horizons is developed to a maximum depth of 1.5 meters (5 ft) in FST2. The Bk horizon, consisting of unit S2(Bk), displayed stage I to stage II carbonate morphology, the latter where the unit overprints unit S1(Bkb) at the east end of the trench. A-horizon thickness ranges from 25 to 100 centimeters (10-40 in).

## Trench FST3

We excavated trench FST3 in a horse pasture in the SE¼ section 14, T. 3 N., R. 1 W., SLBM (figure 5). The trench extended across a broad topographic depression between two high points on a large hummock (figure 10). The trench was approximately 38 meters (125 ft) long and averaged 2 to 2.5 meters (7-8 ft) deep (figure 11). The trench exposed landslide deposits derived from lacustrine sediments (units 1, 2, and 3) similar to those exposed in FST1. High-angle faulting and gentle folding characterized the majority of deformation, although strongly folded beds were present locally. Marker beds indicated 3 to 7 centimeters (1-3 in) of apparent dip slip on individual faults within unit 1 at the north end of the trench. Although these faults appear imbricated on the trench log, their measured strikes (determined by direct measurement of fault surfaces and by correlating faults on opposite trench walls) vary by 76 degrees, indicating the fault planes intersect over relatively small lateral distances. Units 1 and 2 contain several small sand dikes 1 to 7 centimeters (0.4-2.8 in) thick, some of which were injected along fault planes (figure 12). Unit 3 consists of scattered blocks of structureless to brecciated clayey silt that likely represents material from units 1 and 2 that was reworked during landsliding.

Several large, irregular blocks of silty, organic-rich soil comprising unit S1(A) were present near the middle of trench FST3. One of these blocks was truncated by a fault bounding a distinctive horst. These blocks are interpreted to be fragments of one or more soil A horizons that were incorporated into the landslide deposits during landsliding.

A modern soil profile comprising A, Bk, Bt, and Bw horizons is developed to an approximate average depth of 1.3 meters (4 ft) in FST3. A lower Bk horizon consisting of unit S2(Bk2) displayed stage II carbonate morphology and grades upward into a laterally variable B horizon consisting of units S2(Bt), S2(Bk1), and S2(Bw). Unit S2(Bt) is a weakly developed argillic horizon in the middle and topographically lowest part of the trench. This unit grades laterally into unit S2(Bk1), which displayed stage I carbonate morphology. Near the north end of the trench, unit S2(Bk1) also grades laterally into unit S2(Bw), which is a weakly developed cambic horizon. A-horizon thickness ranges from about 20 to 60 centimeters (8-24 in).

## Trench FST4

We excavated trench FST4 on the flank of the southeastern extension of the same large hummock on which FST3 was excavated (figures 5 and 13). Trench FST4 was approximately 20 meters (66 ft) long and averaged 1.5 meters (5 ft) deep (figure 14). The trench exposed landslide deposits derived from lacustrine sediments (units 1, 2, and 3) similar to those exposed in FST1 and FST3. The deposits are dominated by strongly folded, laminated sandy silt and clay (unit 1). Inclined strata consisting of interbedded clay, silt, and sand (unit 2) are juxtaposed against unit 1 along a high-angle fault of uncertain displacement. A fault-bounded blocky deposit (unit 3) con-

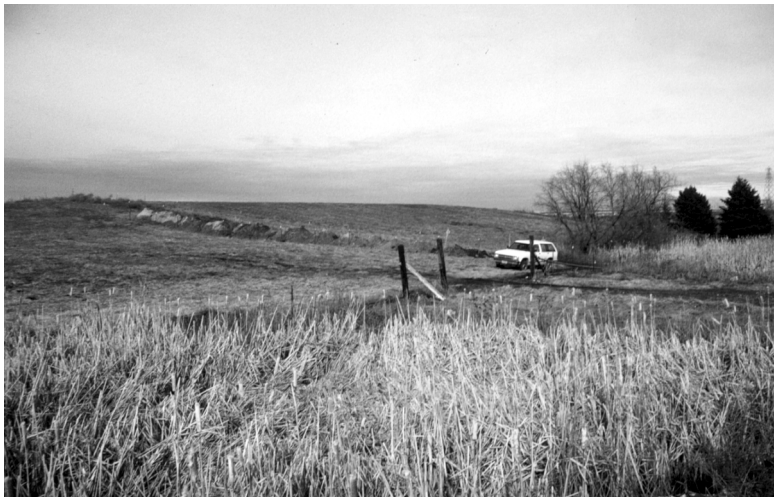

***Figure 8.*** *Trench FST2 (extending up the slope to the left of the vehicle), excavated on the landslide scarp. View is toward the northwest.*




Footnotes:

1 See appendix A for detailed descriptions.

2 See table 2 and appendix B for discussions of analyses and calibrations.

***Figure 9.*** *Log of trench FST2.*

*Figure 10. Trench FST3, excavated between two high points on a large hummock. View is toward the northwest.*

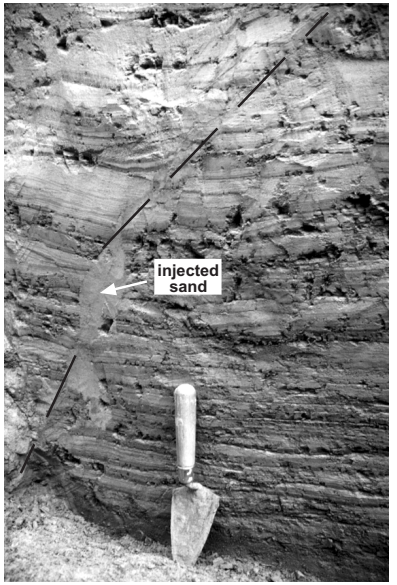


*Figure 12. Liquefied sand injected along fault plane (shown by dashed line) in trench FST3, in east wall at north end of trench. Trowel for scale.*




Footnotes:
1 See appendix A for detailed descriptions.
2 Units with same number on log are lithologically similar but not necessarily stratigraphically equivalent.
3 See table 2 and appendix B for discussions of analyses and calibrations.

*Figure 11. Log of trench FST3.*

Trench FST4
Mapped by M.D. Hylland and B.H. Mayes
December 1994
Planimetric base constructed on a 1 m x 1 m grid
Computer drafted by B.H. Mayes

## EXPLANATION

UNIT DESCRIPTIONS[1]

Modern soil:
S1(A) A horizon
S1(Bw) Bw horizon
S1(Bk) Bk horizon (stage I)

Landslide deposits derived from lacustrine sediment:
3 Yellowish-brown clayey silt with sand and gravel
2 Yellowish-brown interbedded clay, silt, and sand
1 Yellowish-brown sandy silt and clay

SYMBOLS

- A horizon
- Gravel
- Unstratified sand
- Laminae in clay and silt
- Soil-unit boundary
- Intra-unit contact
- Fault, dashed where indistinct (arrows show relative movement)
- Infilled animal burrow
- Bulk-soil radiocarbon sample (age in calendar-calibrated years before present)[2]

***Figure 13***. *Trench FST4, excavated on a hummock sideslope. View is toward the southeast with the Wasatch Range in the background.*

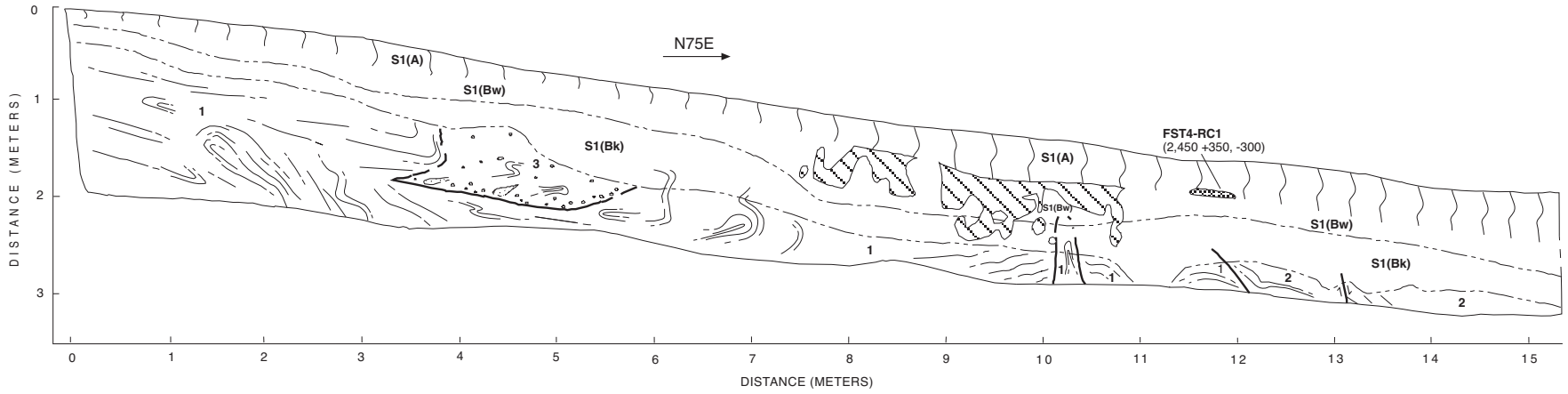


Footnotes:
1 See appendix A for detailed descriptions.
2 See table 2 and appendix B for discussions of analyses and calibrations.

***Figure 14.*** *Log of trench FST4.*

sisting of clayey silt with sand lenses and stringers and scattered gravel is enclosed within unit 1.

A modern soil profile comprising A, Bw, and Bk horizons is developed to depths ranging from 40 to 125 centimeters (16-50 in) in FST4. The Bk horizon, consisting of unit S1(Bk), displayed stage I carbonate morphology and grades upward into a weakly developed cambic horizon consisting of unit S1(Bw). A-horizon thickness ranges from about 13 to 60 centimeters (5-24 in).

### Trench FST5

We excavated trench FST5 in an abandoned field in the NW¼ section 24, T. 3 N., R. 1 W., SLBM (figure 5). FST5 was a composite trench made up of five test pits (A through E) in the area of the boundary between the older and younger landslides identified by Harty and others (1993). The water table was at or just below the ground surface in this area at the time the test pits were excavated (figure 15), and water had to be pumped out of each test pit prior to logging. We used test pits, rather than a single continuous trench, to reduce the volume of water that had to be pumped. Although the surface expression of the landslide boundary has been obscured by agricultural activities, it is relatively distinct on 1952 1:12,000-scale aerial photographs. We established a 25-meter- (80-ft-) wide zone, within which the landslide boundary should be located, relative to cultural features evident on the aerial photographs. The test pits, which were excavated within and on either side of this zone, were each 3.5 to 9 meters (11-30 ft) long (figure 16). The maximum depth of the test pits averaged about 1 meter (3 ft) and was controlled by the depth of caving sands.

Landslide deposits (units 1 and 2) derived from lacustrine sediment were exposed in test pits B, C, D, and E (figure 16). These deposits consist of interbedded clay, sand, and silty sand. The exposure in test pit E indicated that the strata are inclined at least locally. A paleosol consisting of A and weakly developed Bt horizons is present on these landslide deposits. The upper Bt horizon, consisting of unit S1(Bt1), is slightly gleyed as a result of reducing conditions associated with the shallow ground water. Younger landslide deposits (unit 3) overlap the older landslide deposits and paleosol in test pit B. Unit 3 consists of silty fine sand that was unstratified in test pit A, but displayed poorly developed horizontal bedding in test pit B. We interpret this unit to be sand that liquefied and flowed over the surface of pre-existing landslide deposits. The exposure of this unit in test pit B included numerous, variously oriented blocks of dark, organic-rich soil that may be either soil A-horizon fragments incorporated into the landslide deposits or infilled animal burrows.

A modern A horizon 25 to 30 centimeters (10-12 in) thick was present in all of the test pits. This horizon appeared to extend slightly deeper in test pit A. However, the generally uniform depth of the soil and the presence of nearby furrows indicate soil disturbance associated with cultivation.

## SLOPE-FAILURE MODES AND EXTENT OF INTERNAL DEFORMATION

Determining slope-failure modes and the extent of internal deformation within the Farmington Siding landslide complex requires evaluating the geotechnical properties of subsurface materials as well as the geomorphology and structure of the complex and adjacent areas. Specific factors that must be addressed include the liquefaction susceptibility of subsurface materials, the vertical and lateral distribution of materials susceptible to liquefaction, landslide geomorphology, topographic slope, and style(s) of deformation.

### Geotechnical Properties

Because the scope of this project included no subsurface exploration other than relatively shallow trenching, we relied heavily on geotechnical data compiled by Anderson and others (1982) for their liquefaction potential map of Davis County. Anderson and others (1982) compiled logs of geotechnical boreholes at sites between the Wasatch Range and Great Salt Lake, 24 of which are located on or within 1.6 kilometers (1 mi) of the Farmington Siding landslide complex (figure 2). We reviewed the original logs and observed that the deposits involved in slope failure within the landslide complex generally consist of laterally discontinuous layers of clay, silt, sand, and gravel. Based on ground-water depth, grain-size distribution, and standard-penetration-test (SPT) data, Anderson and others (1982) identified liquefiable deposits in the shallow subsurface consisting of very loose to medium dense sand, silty sand, and silt (table 1). These deposits are generally thin bedded, but liquefiable layers of varying thickness are present throughout the shallow subsurface within the landslide complex and in unfailed areas near the margins of the complex.

Subsurface data indicate that the depth to a basal failure surface or liquefiable layer may vary considerably. However, data from the eastern and central parts of the complex may help to locally constrain the depth of a possible failure surface. Anderson and others' (1982) data in the eastern part of the complex indicate that relatively fine-grained deposits consisting of silty sand, silt, and clay with sand interbeds extend to depths of about 9 to 12 meters (30-40 ft) below the ground surface, and are underlain by sand and gravel. Likewise, Miller and others (1981) and Chen and Associates (1988) indicate a similar sequence in the middle part of the complex, where the upper, fine-grained deposits extend to depths ranging from about 4 to 6 meters (14-20 ft). The data also indicate that the upper deposits contain organic matter and have relative densities (based on SPT blow counts) ranging from very loose to medium dense, whereas the lower sand and gravel is medium dense to very dense. A similar sequence is also apparent in unfailed strata east of the eastern margin of the complex, where Anderson and others' (1982) data indicate that loose, fine-grained deposits extend as

***Figure 15.*** *Shallow ground water in test pit C of composite trench FST5. View is toward the east with Interstate-15 overpass in background.*

Trench FST5 (Composite)
Mapped by M.D. Hylland and N.P. Snyder
March - April 1995
Planimetric base constructed on a 1 m x 1 m grid
Computer drafted by B.H. Mayes

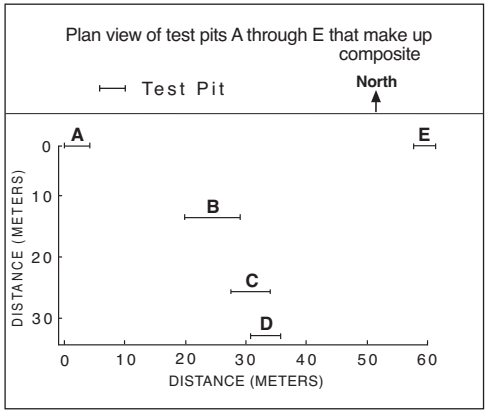


## EXPLANATION

UNIT DESCRIPTIONS[1]

**Modern soil:**
S2(Ap) Cultivated A horizon
S2(A) A horizon

Younger landslide deposit derived from lacustrine sediment:
3 Grayish-brown silty sand

**Paleosol:**
S1(A) A horizon
S1(Bt1) Upper Bt horizon
S1(Bt2) Lower Bt horizon

Older landslide deposits derived from lacustrine sediment:
2 Brown to very dark gray clay with sand
1 Gray to very dark grayish-brown sand and silty sand

SYMBOLS

- A horizon
- Unstratified sand
- Bedding in sand
- Laminae in clay and silt
- Soil-unit boundary
- Geologic contact, dashed where indistinct
- Intra-unit contact
- Infilled animal burrow
- Bulk-soil radiocarbon sample (age in calendar-calibrated years before present)[2]

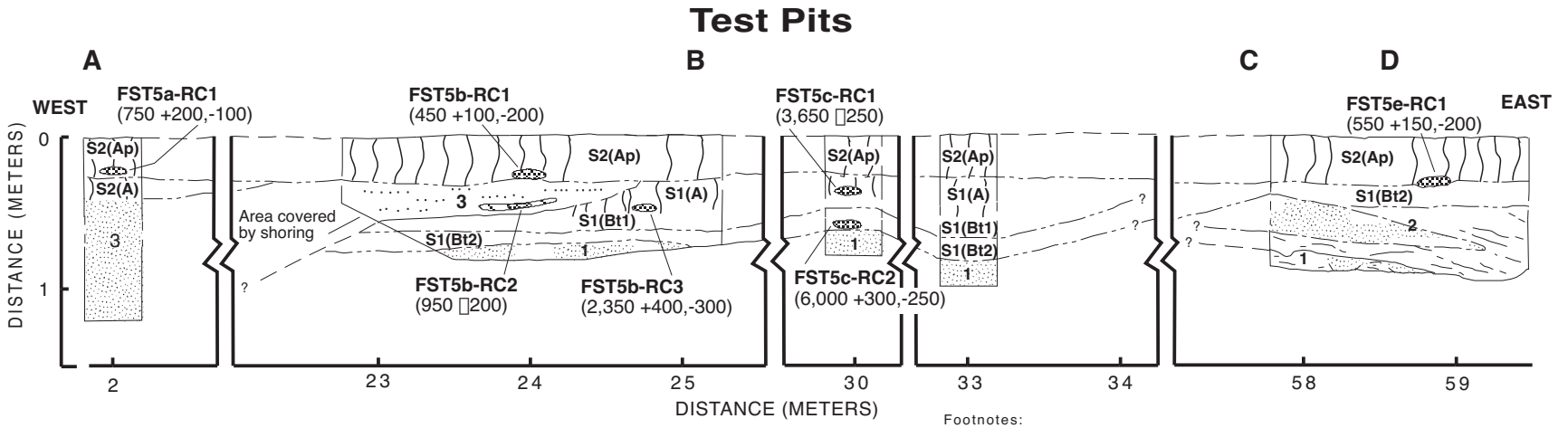


Footnotes:
1 See appendix A for detailed descriptions.
2 See table 2 and appendix B for discussions of analyses and calibrations.

***Figure 16.*** *Log of trench FST5 and plan view showing locations of test pits that make up the composite trench.*

***Table 1.***
*Subsurface geotechnical properties within and near the Farmington Siding landslide complex.*

| | | | Liquefiable Deposits | | | |
|---|---|---|---|---|---|---|
| **Site No.[1]** | **Borehole Depth (m)[2]** | **Ground-Water Depth (m)** | **USCS** | $N_{min}$ | $\overline{N}$ | $a_c$ **(g)** |
| 1 | 10.4 | 2.3 | SP, SM, ML | 9 | 13 | 0.16 |
| 2 | NA | 1.5 | NA | NA | NA | NA |
| 3 | 38.7 | 3.9 | SP, SM, ML | 6 | 25 | 0.12 |
| 4 | 9.6 | 2.4 | SP | 14 | 31 | 0.20 |
| 5 | 14.2 | 0.8 | SM, ML | 5 | 14 | 0.12 |
| 6 | 12.2 | 1.0 | SP, SM, ML | 4 | 11 | 0.09 |
| 7 | 12.5 | 0.6 | SP, SM, ML | 10 | 10 | 0.15 |
| 8 | 20.5 | NA | SP, SM | NA | NA | NA |
| 9 | 12.2 | 2.0 | SP, SM, ML | NA | NA | NA |
| 10 | 18.6 | 0.3 | SP, SM | NA | NA | NA |
| 11 | 8.8 | 0.8 | SM | NA | NA | NA |
| 12 | 9.6 | 1.2 | SP, SM, ML | 5 | 8 | 0.08 |
| 13 | 22.0 | 0.0 | SM, ML | 4 | 10 | 0.07 |
| 14 | 30.5 | 0.0 | SM, ML | 4 | 12 | 0.07 |
| 15 | 26.5 | 0.5 | SP, SM, ML | 3 | 8 | 0.06 |
| 16 | 4.6 | 1.1 | SM, ML | NA | NA | NA |
| 17 | 9.5 | 0.3 | SP, SM, ML | 2 | 18 | 0.05 |
| 18 | 27.5 | 2.2 | SP, SM | 10 | 30 | 0.10 |
| 19 | 16.9 | 2.0 | SP, SM, ML | 3 | 6 | 0.05 |
| 20 | 30.5 | 0.0 | SP, SM, ML | 2 | 2 | 0.05 |
| 21 | NA | 0.2 | NA | 12 | 30 | 0.13 |
| 22 | 30.5 | 1.2 | SP, ML | 11 | 23 | 0.13 |
| 23 | 23.5 | 2.0 | SP, SM | 15 | 19 | 0.16 |
| 24 | 7.5 | 4.0 | SP, SM, ML | 3 | 3 | 0.10 |

[1]*Sites are re-numbered from Anderson and others (1982); see figure 2 for locations.*

[2]*Depth is a maximum depth if more than one hole was drilled at a site.*

*Abbreviations: USCS = Unified Soil Classification System;* $N_{min}$ *= minimum SPT blow counts;* $\overline{N}$*= average SPT blow counts;* $a_c$ *= critical acceleration; NA = data not available.*

deep as 20 meters (65 ft) and are underlain by dense sand and gravel. Borehole logs indicate the top of the medium-dense to very dense sand and gravel ranges in elevation between about 1,268 and 1,289 meters (4,158-4,227 ft). These elevations are below the elevation of the Stansbury shoreline, which formed during the transgressive phase of Lake Bonneville (Currey and others, 1983; Green and Currey, 1988; Oviatt and others, 1990). These deposits, therefore, may represent a transgressive lacustrine sequence consisting of relatively dense nearshore sand and gravel deposited during the early part of the Bonneville paleolake cycle, or possibly pre-Bonneville alluvium, overlain by loose/soft, offshore, fine-grained sediments subsequently deposited in deeper water. The contact between these different depositional facies of contrasting density and shear strength may correspond at least locally to a landslide failure surface.

## Geomorphology

The existence in the northern part of the landslide complex of a main scarp with up to 12 meters (40 feet) of relief indicates flow was a significant slope-failure mode. Such a scarp would not result from lateral spread alone. Other evidence for flow failure includes: the hummocky topography; the overall negative relief in the head region of the complex, indicating evacuation of a large volume of material; and the overall positive relief in the distal region of the complex, indicating an accumulation of landslide material.

Harty and others (1993) mapped an area of transverse lineaments near the middle of the landslide complex that may represent infilled ground cracks associated with lateral spread. Although these lineaments could also represent shorelines formed during post-Gilbert regression of Great Salt Lake (Lowe and others, 1995), three features of the lineaments support a landslide origin. First, the lineaments are preserved on the northern (younger) part of the complex, but not on the southern part. Depending on the timing of shoreline development relative to landsliding, shorelines should be preserved either across the entire complex or only on the southern part. Second, several of the lineaments display an anastomosing pattern uncharacteristic of shorelines. Third, lineaments adjacent to the southeast boundary of the northern landslide are consistently convex in the downslope direction and terminate along the boundary. This pattern indicates the lineaments likely formed during movement of the northern landslide and were drag-folded by differential movement near the landslide margin.

Unfailed slopes along the flanks of the landslide complex, which approximate the pre-failure slopes within the complex, are within the typical range of 0.5 to 5 percent (0.3-3 degrees) for documented lateral spreads (Youd, 1978, 1984; National Research Council, 1985). The combination of topographic slope and locally conducive stratigraphy indicates that lateral spread would be an expected failure mode. However, flow failure has been documented on slopes as low as 2.3 degrees (Keefer, 1984). Based purely on slope, therefore, flow failure could have occurred locally, especially near the head of the complex where pre-failure slopes were likely steeper. By excavating trenches across hummock flanks and adjacent ground in the northern part of the complex, Harty and others (1993) determined the hummocks are relatively intact "islands" of lacustrine strata surrounded by liquefied sand, and concluded that flow failure had occurred in this part of the complex. Also, the nature of deposits exposed in trench FST3 provides additional evidence for flow failure. Unit 1 of trench FST3 consists of cyclically bedded sand and clayey silt that was very similar in appearance to lacustrine strata exposed in a road cut along Swinton Lane in the landslide main scarp approximately 1.8 kilometers (1.2 mi) north of the trench (figures 3 and 5). In contrast, unit 1 did not resemble any of the scarp material exposed in trench FST2, approximately 0.5 kilometer (0.3 mi) northwest of trench FST3. Therefore, the hummock on which trench FST3 was excavated may have been displaced southward a considerable distance, possibly as much as a kilometer or more, from its original location. This likely could only have been achieved by flow transport during one or more flow-failure events.

## Structure

The trench exposures revealed several contrasting styles of deformation: ductile or plastic deformation characterized by strong folding; brittle deformation characterized by discrete, nondisrupted, low-angle faulting; brittle deformation characterized by high-angle faulting; and flow characterized by disruption or loss of internal structure (figure 17). Some deformation likely predates subaerial landsliding within the complex. This deformation includes convolute lamination and recumbent, isoclinal folds exhibited in trenches FST3 and FST4, and low-angle faults in trench FST1. The nature of these structures indicates they were formed under subaqueous conditions, or possibly during subaerial landsliding but at a depth unaffected by surficial disturbance and under relatively high confining pressures. In the latter case, extensive erosion would have been necessary to result in the present shallow depth of these deposits. This does not seem likely, given the low regional topographic gradient and the relatively fresh geomorphic appearance of the hummocks within which the structures occur. Also, these structures closely resemble folds and faults exposed in a road cut along Main Street north of downtown Farmington (figure 18), east of the landslide main scarp and therefore not involved in landsliding within the complex. These structures likely represent penecontemporaneous deformation associated with slumping beneath Lake Bonneville that predates subaerial landsliding.

High-angle faults involving organic soil units were encountered in trenches FST2 and FST3 (figure 19) and are clearly associated with subaerial landsliding. The nature of the faults exposed in trench FST2 indicates that

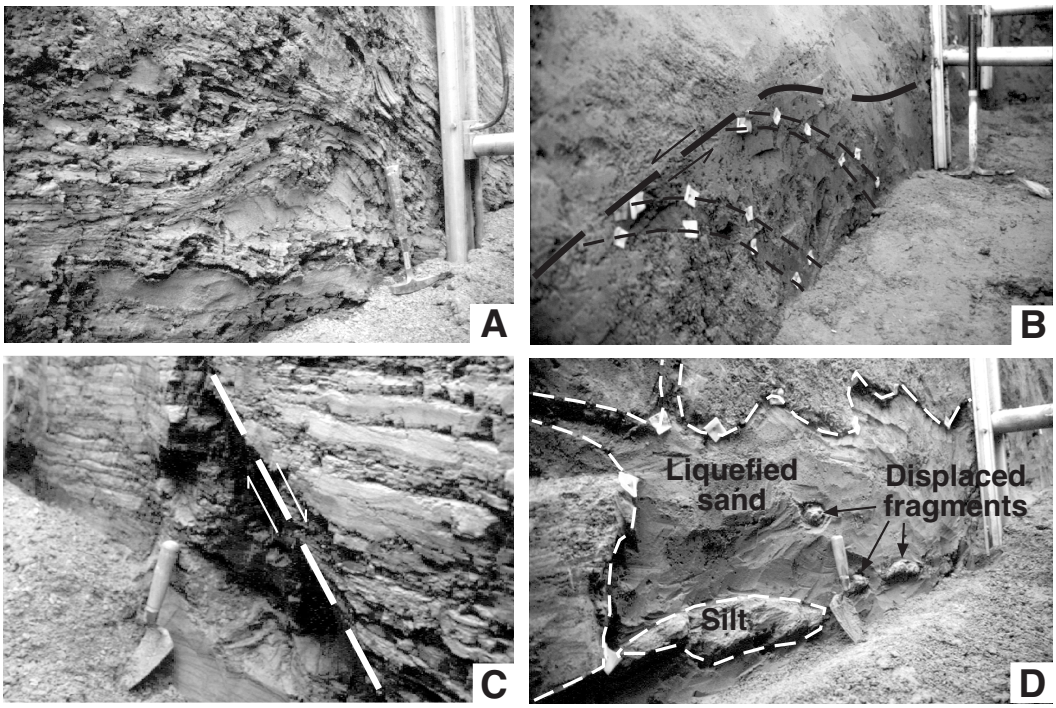


***Figure 17***. *Styles of deformation in landslide deposits in the Farmington Siding landslide complex. A) Ductile deformation characterized by strong folding in thin-bedded sand and silt in trench FST3; hammer for scale. B) Brittle deformation characterized by low-angle faulting in trench FST1; hammer for scale. Fault trace (marked by heavy dashed line with arrows showing relative movement) truncates gentle folds (marked by flagging squares); trenching tool for scale. C) Brittle deformation characterized by high-angle faulting in trench FST3. Shadowed area is adjacent to exhumed surface of fault (marked by heavy dashed line with arrows showing relative movement); trowel for scale. D) Flow of liquefied sand in trench FST2. Disruption of silt interbed (left of trowel) is indicated by detached and displaced fragments (above and right of trowel).*

***Figure 18.*** *Folded lacustrine strata exposed in a road cut along Main Street north of downtown Farmington (see figure 5 for location). Exposure is east of the Farmington Siding landslide complex, and therefore deposits were not involved in landsliding within the complex. Trowel in center of photo for scale.*

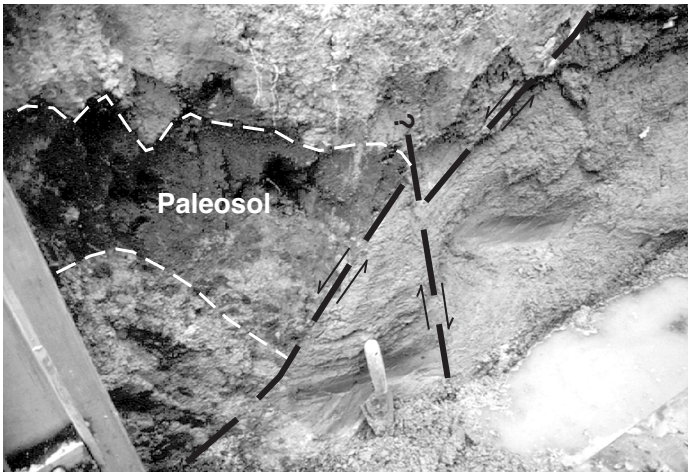


***Figure 19.*** *High-angle fault (marked by heavy dashed line with arrows showing relative movement) involving organic soil unit in trench FST3. Fault juxtaposes paleosol A horizon (dark material) against lacustrine strata (lighter material).*

rotational or translational block sliding may have played a significant role in scarp formation. The dominant style of deformation in trench FST3 is extensional, as indicated by numerous normal faults and horst-and-graben structures. These features appear to be related to internal deformation of the hummock during landsliding. Although displacements on most of these faults were on the order of a few centimeters, A-horizon soil blocks were downdropped to a depth of about 2 meters (7 ft) near the middle of the trench.

Trenches FST2, FST3, and FST5 showed evidence for flow of liquefied sand. In trench FST2, subhorizontal fragments of silt within a structureless sand bed indicate at least one formerly continuous silt interbed was attenuated and disrupted as the sand liquefied. Lateral extension of the sand would likely have been accompanied by subsidence of the overlying strata, which together with vertical displacement along scarp-forming slip surfaces produced the overall topographic expression of the scarp. Small sand dikes were present in trenches FST2 and FST3, indicating minor lateral spread of silt and clay beds over liquefied sand. In trench FST5, surficial liquefied sand flowed over pre-existing landslide deposits.

## LANDSLIDE TIMING

Relative and absolute dating techniques used to determine the timing of landsliding include: geomorphic expression of landslide features; cross-cutting relations of landslide boundaries and Great Salt Lake shorelines; soil-profile development on landslide deposits; and radiocarbon dating of organic soils developed on and incorporated into the landslide deposits.

### Geomorphic Expression of Landslide Features

Harty and others (1993) concluded that major movement on the southern part of the landslide complex is appreciably older than that on the northern part of the complex based on the abundance and distinctiveness of geomorphic features, especially hummocks, on the northern part. Variation in the slope of the landslide main scarp also supports this conclusion, as the southern part of the scarp appears to have eroded to a much gentler slope than the northern part.

### Great Salt Lake Shorelines

Van Horn (1975) noted that landsliding in the northern part of the complex truncated the Gilbert shoreline, which formed between 10,900 and 10,300 $^{14}$C yr B.P. (Currey, 1990), indicating major post-Gilbert movement. Anderson and others (1982) and Harty and others (1993) mapped the Gilbert shoreline across the southern part of the complex (although in different places), indicating pre-Gilbert landsliding in this part of the complex. Aerial-photograph review during this study confirmed the presence of an apparent shoreline feature at an elevation of approximately 1,293 meters (4,240 ft) on the southeastern part of the complex that could represent the Gilbert highstand. The northwestern continuation of this feature in the middle part of the complex is evident but difficult to trace, possibly due to disruption by relatively minor post-Gilbert landsliding.

Harty and others (1993) mapped shorelines on the southern part of the landslide complex (figure 2) near an elevation of 1,287 meters (4,221 ft), which is the elevation of the Holocene highstand of Great Salt Lake between about 2,500 and 1,400 $^{14}$C yr B.P. (Currey and others, 1988; Murchison, 1989; Currey, 1990). These shorelines are not evident on the northern part of Harty and others' (1993) southern landslide or on their northern landslide, indicating possible landsliding since about 1,400 years ago of sufficient magnitude to disrupt the shorelines. Alternatively, the original geomorphic expression of the shorelines may have been subtle relative to pre-existing landslide geomorphology, making the shorelines difficult to recognize, or the shorelines have been obscured by grading or agricultural activities.

Harty and others (1993) mapped shorelines on both the southern and northern parts of the landslide complex (figure 2) near an elevation of 1,286 meters (4,215 ft), which is the elevation of the late-prehistoric highstand of Great Salt Lake around A.D. 1,600-1,700 (Murchison, 1989; Currey, 1990). The presence of these shorelines indicates that major, ground-disrupting landsliding has not affected the distal parts of the complex during the past approximately 400 years.

### Soil-Profile Development

Soil-profile development can provide information on the relative timing of landsliding. In general, a relatively deep, well-developed soil profile on landslide deposits may indicate a relatively long period of landscape stability. However, soil survey information (Erickson and Wil-

son, 1968) documents wide variability in morphology and degree of development of surficial soils on and in the vicinity of the Farmington Siding landslide complex. This variability, which is typical of late Quaternary surficial soils along the Wasatch Front, is due more to microclimatic conditions and the physical characteristics of the parent material than to the age of the parent material (Shroba, 1980).

Perhaps the most useful applications of soil-horizon development, in particular clay enrichment and accumulation of secondary calcium carbonate, to determining landslide timing are in differentiating surfaces that likely existed prior to landsliding from surfaces created during landsliding, and providing a context within which to interpret radiocarbon ages. For example, profiles with argillic Bt horizons may be associated with surfaces at least as old as early Holocene (Scott and Shroba, 1985), and Bk horizons displaying stage II carbonate morphology may be associated with similarly old surfaces. Bt and stage II Bk horizons were observed only in trenches FST2, FST3, and FST5. In the case of trench FST2, the Bk horizon is faulted and buried beneath undisrupted colluvial soil with stage I carbonate morphology. These relations indicate a relatively long period of soil development followed by scarp-forming landsliding, in turn followed by landscape stability. The presence of Bt and stage II Bk horizons in trench FST3 may indicate either early Holocene soil development that postdates hummock deformation, or preservation of a soil profile that predates landsliding. Development of Bt horizons on old landslide deposits in trench FST5 indicates a lack of significant late Holocene ground disturbance. In contrast, the maximum stage I carbonate morphology in the soils in trenches FST1 and FST4 indicates a relatively shorter period of pedogenesis, and therefore a more recent period of significant ground disturbance.

## Radiocarbon Ages

Bulk-sediment samples were obtained from the trenches during this study for radiocarbon age determinations. Table 2 summarizes the radiocarbon age data, and appendix B provides information regarding radiocarbon analyses and calendar calibrations. All radiocarbon ages discussed in this section are designated as $^{14}$C yr B.P. and are listed with a laboratory identification number. Elsewhere in this report, radiocarbon ages are designated as $^{14}$C yr B.P. and calendar-calibrated ages are designated as cal yr B.P.

Radiocarbon dating of organic soils developed on and incorporated into landslide deposits can provide absolute information on the timing of landsliding, although the results may not closely date specific landslide events. To closely date a flow-failure or lateral-spread event, a sample is needed from the upper part of an organic soil horizon that has been buried by deposits produced during landsliding (such as flow or sand-blow deposits). Except for flow deposits overlying a paleosol on older landslide deposits in trench FST5, we did not encounter these kinds of stratigraphic relations in the trenches. The organic soils that were sampled for radiocarbon dating were generally modern A-horizon soils and paleosol fragments incorporated into the landslide deposits. Thus, we interpret the ages obtained for these soils as representing minimum and maximum limiting ages, respectively, of landsliding.

The oldest ages (8,350 ± 80 [Beta-80453] and 7,480 ± 70 [Beta-80454] $^{14}$C yr B.P.) we obtained were from paleosol blocks of unit S1(A) in trench FST3. The incorporation of these paleosol blocks in landslide deposits to depths of about 2 meters (7 ft) indicates significant disruption of the former ground surface. The soil ages represent a maximum limiting age for a landslide event of about 7,480 $^{14}$C yr B.P., assuming the blocks represent parts of the same soil profile disturbed during a single landslide event; this interpretation is favored based on the physical similarities of the paleosol blocks and their relative positions in the trench wall. The landslide could have occurred up to several thousand years later than this limiting age, depending on the age of the soil at the time it was incorporated into the landslide deposits. Given the relatively old ages of the soils and the fact that they are overprinted by a relatively well-developed modern soil profile (stage II carbonate morphology), landsliding sometime during the early to middle Holocene seems likely.

The base of the colluvial wedge (unit 3) in trench FST2 yielded an age of 7,310 ± 60 $^{14}$C yr B.P. (Beta-80450). This age represents a maximum limiting age for the onset of colluvial-wedge deposition. Therefore, an episode of landslide scarp formation likely occurred at this location shortly before this time. At least one subsequent episode of scarp modification associated with landsliding is indicated by the offset of the buried stage II carbonate horizon consisting of unit S1(Bkb). However, the age of 3,650 ± 70 $^{14}$C yr B.P. (Beta-80451) from the base of the modern A horizon in trench FST2 indicates relative ground-surface stability at this location on the scarp during the late Holocene. Any landsliding subsequent to early Holocene scarp formation appears not to have created a new scarp in this area.

Unit S1(Bt2) in trench FST5 yielded an age of 5,280 ± 60 $^{14}$C yr B.P. (Beta-81833). Because this unit is at the base of the soil profile developed on older landslide deposits, we interpret the age as indicating relative stability of this area during the late Holocene. Although the soil may have developed on an isolated geomorphic feature (for example, a hummock) that has remained stable during late Holocene landsliding relative to the landslide mass as a whole, the locally flat topography makes this unlikely. The base of unit S1(A) in trench FST5 yielded ages of 3,390 ± 50 (Beta-81832) and 2,340 ± 60 (Beta-81831) $^{14}$C yr B.P. This unit represents the A horizon of this paleosol and is unconformably overlain by younger landslide deposits (unit 3). Although the cause of the difference in ages is uncertain, the ages indicate the soil was buried by the younger landslide deposits sometime after about 2,340 $^{14}$C yr B.P. or less, depending on the soil age at the time of

***Table 2***.
*Radiocarbon age estimates on bulk sediment from the Farmington Siding landslide complex*.

| Sample (Lab ID) | Sample Source[1] | Conventional $^{14}C$ Age[2,3] yr B.P. | Calendar-Calibrated Age[4], yr B.P., ± 2σ (2σ intercept ranges) |
|---|---|---|---|
| FST2-RC1 (Beta-80450) | Trench FST2, base of unit 3 (colluvial paleosol) | 7,310 ± 60 | 8,100 + 250, -200 (8,350-7,900) |
| FST2-RC2 (Beta-80451) | Trench FST2, base of unit S2(A) (modern A horizon) | 3,650 ± 70 | 3,950 + 450, -350 (4,400-3,600) |
| FST3-RC1 (Beta-80452) | Trench FST3, base of unit S2(A) (modern A horizon) | 1,200 ± 40 | 1,100 + 200, -150 (1,300-950) |
| FST3-RC2 (Beta-80453) | Trench FST3, middle of unit S1(A) block (paleosol) | 8,350 ± 80 | 9,400 + 200, - 450 (9,600-8,950) |
| FST3-RC3 (Beta-80454) | Trench FST3, middle of unit S1(A) block (paleosol) | 7,480 ± 70 | 8,300 + 200, -300 (8,500-8,000) |
| FST4-RC1 (Beta-80455) | Trench FST4, base of unit S1(A) (modern A horizon) | 2,440 ± 70 | 2,450 + 350, - 300 (2,800-2,150) |
| FST5a-RC1 (Beta-81828) | Trench FST5 (test pit A), base of unit S2(Ap) (modern A horizon, disturbed) | 840 ± 50 | 750 + 200, - 100 (950-650) |
| FST5b-RC1 (Beta-81829) | Trench FST5 (test pit B), base of unit S2(Ap) (modern A horizon, disturbed) | 370 ± 50 | 450 + 100, - 200 (550-250) |
| FST5b-RC2 (Beta-81830) | Trench FST5 (test pit B), middle of thin organic-rich soil within unit 4 (likely infilled animal burrow) | 1,050 ± 50 (AMS)[5] | 950 ± 200 (1,150-750) |
| FST5b-RC3 (Beta-81831) | Trench FST5 (test pit B), base of unit S1(A) (paleosol A horizon) | 2,340 ± 60 | 2,350 + 400, - 300 (2,750-2,050) |
| FST5c-RC1 (Beta-81832) | Trench FST5 (test pit C), base of unit S1(A) (paleosol A horizon) | 3,390 ± 50 | 3,650 ± 250 (3,900-3,400) |
| FST5c-RC2 (Beta-81833) | Trench FST5 (test pit C), base of unit S1(Bt2) (paleosol B horizon) | 5,280 ± 60 | 6,000 + 300, - 250 (6,300-5,750) |
| FST5e-RC1 (Beta-81834) | Trench FST5 (test pit E), base of unit S2(Ap) (modern A horizon, disturbed) | 540 ± 60 | 550 + 150, - 200 (700-350) |

[1]*Refer to appendix A for detailed descriptions of sample source material*.

[2]*All ages* $\delta^{13}C$ *corrected*.

[3]*All ages determined by standard radiometric analysis unless otherwise noted; see appendix B*.

[4]*Calibrated using methods of Stuiver and Reimer (1993); see appendix B*.

[5]*Accelerator mass spectrometry*.

burial. A dark, organic-rich soil fragment within unit 3 yielded an age of 1,050 ± 50 $^{14}$C yr B.P. (Beta-81830), and is likely an infilled animal burrow as opposed to a fragment of the overridden paleosol A horizon.

Of the remaining ages obtained from the base of the modern A-horizon soils in trenches FST3, FST4, and FST5, only the age of 2,440 ± 70 $^{14}$C yr B.P. (Beta-80455) from trench FST4 was likely not affected by modern human activity. This age may indicate surface disruption just prior to about 2,440 yr B.P. and relative stability since that time. The other ages, which range from 370 ± 50 (Beta-81829) to 1,200 ± 40 (Beta-80452) $^{14}$C yr B.P. (see table 2), are from relatively thin A horizons in previously cultivated areas where the bottom of the horizon may have been contaminated by mechanical mixing with young carbon and possible soil additives used in agriculture.

## Episodes of Landsliding

In summary, relative and absolute timing information indicates at least three, and possibly four, landslide events in different parts of the Farmington Siding landslide complex (figure 20). The earliest event occurred after deposition of Provo-aged Lake Bonneville sediments but before formation of the Gilbert shoreline (Harty and others, 1993), and therefore between about 14,500 and 10,900 $^{14}$C yr B.P. (Currey, 1990). This event involved at least the extreme southern part of the complex, but its northern extent is unknown because it has been obscured by subsequent landslides.

A second event occurred just prior to 8,100 (+250, -200) cal yr B.P., based on the calendar-calibrated maximum limiting age of the onset of colluvial-wedge deposition on the landslide scarp. This event involved at least the northwestern part of the complex (figure 20), and probably incorporated A-horizon soils into the landslide deposits encountered in trench FST3. A possible third event may have occurred sometime before 6,000 (+300, -250) cal yr B.P., based on the calendar-calibrated maximum limiting age associated with the onset of soil-profile development on landslide deposits near the middle of the complex. Depending on surface and climate conditions, however, the inception of pedogenesis may not provide a close limiting age for this landslide event. The southeastern margin of this landslide, which involved at least the middle part of the complex (figure 20), corresponds to the boundary between the two landslides mapped by Nelson and Personius (1993) in the southern part of the complex. The landsliding in this area could alternatively have been distal movement associated with the pre-8,100 cal yr B.P. event, rather than a separate event. In either case, movement in this area was not sufficiently large to completely destroy the geomorphic expression of the Gilbert shoreline.

A fourth event occurred sometime between 2,750 and 2,150 cal yr B.P. This interval is based on the maximum and minimum two-sigma error limits, respectively, of calendar-calibrated ages associated with a pre-existing soil dated at 2,340 ± 60 $^{14}$C yr B.P. (Beta-81831) at trench FST5 that was overridden by landslide deposits (maximum limiting age of 2,350 [+400] cal yr B.P.), and post-landslide soil development dated at 2,440 ± 70 $^{14}$C yr B.P. (Beta-80455) on the hummock slope at trench FST4 (minimum limiting age of 2,450 [-300] cal yr B.P.). This event involved the northern and western parts of the complex (figure 20). A new main scarp likely formed as the result of headward migration to the northeast, whereas the exist-

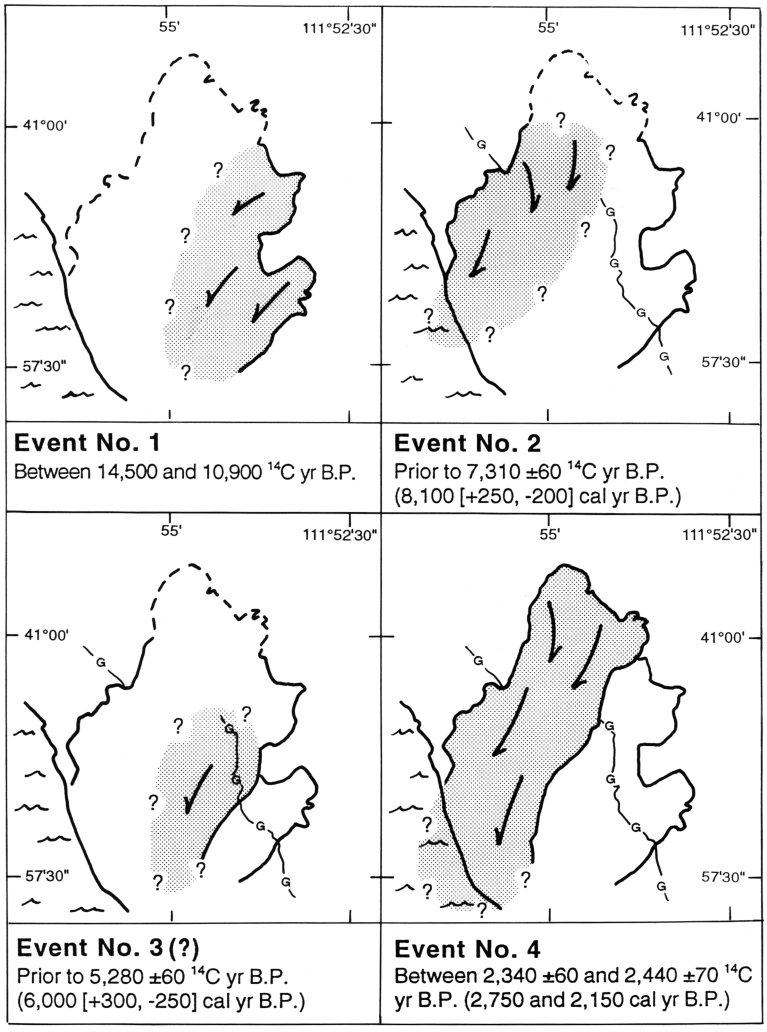


***Figure 20.*** *Generalized areas of landsliding (shaded areas) within the Farmington Siding landslide complex during four events indicated by geomorphic expression of landslide features, cross-cutting relations of lake shorelines, and soil radiocarbon ages. Solid line indicates relatively well-constrained boundary formed during landslide event, dashed line indicates present main-scarp position, queried boundary indicates uncertain extent. Arrows show speculated direction of landslide movement. Landslide-complex boundary and Gilbert shoreline (lineament with "G" designation) from Harty and others (1993). Present shoreline of Farmington Bay shown for reference.*

ing scarp at the location of trench FST2 apparently acted as a lateral scarp during this event. The timing of this event determined in this study corresponds well with Harty and others' (1993) bracketing ages of 4,530 ± 300 and 2,730 ± 370 cal yr B.P. for movement on their northern landslide, and reasonably well with the radiocarbon age of 2,930 ± 70 $^{14}$C yr B.P. from organic mud on the toe of the landslide beneath Farmington Bay (Everitt, 1991).

## GEOLOGIC/HYDROLOGIC CONDITIONS DURING LANDSLIDING

Inferences regarding geologic and hydrologic conditions during landsliding at the Farmington Siding landslide complex can be made by combining topographic, stratigraphic, and landslide-timing data with postulated ground-water conditions associated with paleoclimatic changes and lacustral fluctuations of Lake Bonneville and Great Salt Lake. The Bonneville basin was characterized by closed-basin hydrology throughout most of the Quaternary. Following the Provo stage of Lake Bonneville, during which the high lake level allowed extra-basinal drainage via the Snake and Columbia Rivers, climatic conditions forced a reversion to closed-basin hydrology after about 14,000 $^{14}$C yr B.P. (Currey and Oviatt, 1985). Changes in ground-water levels and associated soil pore-water pressures, and therefore changes in susceptibility to landsliding in lake-margin areas, can be deduced from periods of climate-controlled lacustrine contractions and expansions. Therefore, summaries of late Quaternary climatic and lacustral conditions (for example, Madsen and Currey, 1979; Currey and James, 1982; Murchison, 1989; Rhode and Madsen, 1995) provide a useful context within which to reconstruct conditions during landslide events.

Lake Bonneville, of which Great Salt Lake is a remnant, occupied the Bonneville basin between about 30,000 and 12,000 $^{14}$C yr B.P. (Oviatt and others, 1992). The Bonneville paleolake cycle was the last of several Pleistocene deep-lake cycles in the Bonneville basin (McCoy, 1987; Oviatt and Currey, 1987) and ended when the lake regressed to a lowstand, marked locally by mirabilite and red beds (Eardley, 1962; Currey, 1990), after about 12,000 $^{14}$C yr B.P. (Oviatt and others, 1992; Rhode and Madsen, 1995). During the subsequent Gilbert transgression, Great Salt Lake reached its highest stage between 10,900 and 10,300 $^{14}$C yr B.P. (Currey, 1990; Oviatt and others, 1992). The timing of pre-Gilbert landsliding within the Farmington Siding landslide complex is poorly constrained, and may have occurred as subaqueous slumping beneath Lake Bonneville or subaerial landsliding near the end of the Lake Bonneville regression when the gently sloping, saturated lacustrine sediments were draining. Alternatively, landsliding could have occurred when lake and ground-water levels (and associated pore-water pressures) were rising during the Gilbert transgression.

After regression from the Gilbert highstand to near the historic mean elevation of 1,281 meters (4,200 ft) (Murchison, 1989), Great Salt Lake again transgressed to an elevation of about 1,284 meters (4,213 ft) between about 7,300 and 7,100 $^{14}$C yr B.P. (Murchison, 1989). This time period coincides with the second Farmington Siding landslide event that occurred prior to 7,310 ± 60 $^{14}$C yr B.P. (or 8,100 cal yr B.P.). The topographic expression of the preserved Gilbert shoreline northwest of the landslide complex indicates that the shoreline may have contributed to landsliding by acting as a free face along which a failure surface could have initiated.

Palynologic data indicate a relatively warm and dry climate between about 8,000 and 6,000 $^{14}$C yr B.P. (Madsen and Currey, 1979), and Great Salt Lake regressed to near desiccation levels during this time (Currey, 1980; Murchison, 1989). The climate then became wetter between about 6,000 and 3,500 $^{14}$C yr B.P. (Madsen and Currey, 1979). Murchison (1989) reports a lake-level rise to 1,283 meters (4,211 ft) around 5,900 $^{14}$C yr B.P., which is near the age of the possible third landslide event that may have occurred prior to about 5,280 ± 60 $^{14}$C yr B.P. (or 6,000 cal yr B.P.).

After about 3,500 $^{14}$C yr B.P., precipitation declined to near the Holocene average and temperatures declined to below the Holocene average (Madsen and Currey, 1979). Great Salt Lake began a relatively major transgression around 3,440 $^{14}$C yr B.P. (Murchison, 1989), possibly the result of reduced evapotranspiration. This transgression culminated in the Holocene highstand at an elevation of 1,287 meters (4,221 ft) between about 2,500 and 1,400 $^{14}$C yr B.P. (Currey and others, 1988; Murchison, 1989). This lacustral highstand coincides with the fourth Farmington Siding landslide event that occurred sometime around 2,340 ± 60 to 2,440 ± 70 $^{14}$C yr B.P. (or between limiting ages of about 2,750 and 2,150 cal yr B.P.). The apparent correspondence throughout the late Quaternary between landslide events and lacustral highstands supports the hypothesis that landsliding occurred under conditions of relatively elevated ground-water levels and soil pore-water pressures associated with high lake levels.

## SEISMIC CONSIDERATIONS

Obermeier (1987) and Obermeier and others (1990) have developed criteria for establishing an earthquake origin for liquefaction-induced features. The criteria include various characteristics of sand blows, the presence of lateral spreads, possible mechanisms of sedimentary dike and sill formation, mechanical properties of near-surface sediment, and the potential for strong ground shaking at the site. Many of the features associated with the Farmington Siding landslide complex (for example, evidence of lateral spread, sand dikes, deposits susceptible to liquefaction) indicate landsliding could have been triggered by strong ground shaking.

Many earthquake source zones exist in northern Utah, and we conclude that certain of these source zones could produce earthquakes that generate ground shaking of suf-

ficient strength and duration to trigger large-scale liquefaction-induced landsliding at the Farmington Siding landslide complex. Our conclusion is based on five independent means of evaluation: (1) empirical earthquake magnitude-distance relations, (2) comparison of expected peak horizontal ground accelerations with calculated critical accelerations, (3) liquefaction severity index, (4) estimated Newmark landslide displacements, and (5) comparison of landslide timing with fault-zone paleoseismicity.

## Earthquake Magnitude-Distance Relations

Proximity to earthquake source zones and earthquake magnitudes associated with those source zones are two factors important in evaluating earthquakes as possible triggering mechanisms for liquefaction-induced landslides. Figure 21 shows mapped fault zones nearest to the Farmington Siding landslide complex with evidence for Holocene activity; these include the East Cache, East Great Salt Lake, West Valley, Oquirrh, and Wasatch fault zones (Hecker, 1993). Maximum earthquake magnitudes, based on rupture-length, surface-displacement, and slip-rate parameters, are about surface-wave magnitude ($M_s$) 7.1 for the central segment of the East Cache fault zone (McCalpin, 1994), moment magnitude ($M_w$) 7.0 for the East Great Salt Lake and Oquirrh fault zones (Hecker, 1993; Olig and others, 1996), $M_w$ 6.7 for the West Valley fault zone (Keaton and others, 1987), and $M_w$ 6.9 - 7.4 for the six active central segments of the Wasatch fault zone (Youngs and others, 1987; Machette and others, 1991; Black and others, 1995, 1996). For consistency in the following analyses, the maximum earthquake on the East Cache fault zone is taken to be $M_w$ 7.1; $M_w$ approximately equals $M_s$ at this magnitude (Kanamori, 1983).

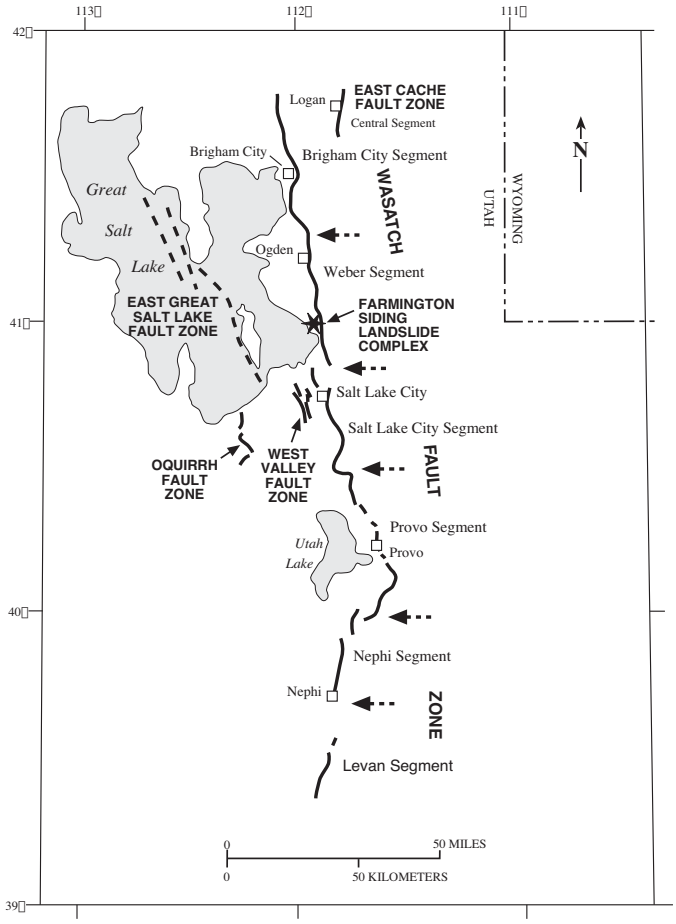


***Figure 21***. *Fault zones in the vicinity of the Farmington Siding landslide complex with evidence for Holocene movement (modified from Arabasz and others, 1992; Machette and others, 1992; Hecker, 1993). Wasatch-fault-zone segments designated with lower-case script; arrows show segment boundaries.*

Keefer (1984) compiled worldwide data from a variety of geologic and seismic settings on the maximum distance of lateral spreads and flows from earthquake epicenters and fault-rupture zones relative to earthquake magnitude. Figure 22 shows Keefer's (1984) empirically derived curve indicating maximum distance of lateral spreads and flows from fault-rupture zones, as well as possible maximum distances to lateral spreads and flows triggered by maximum earthquakes on the East Cache, East Great Salt Lake, West Valley, Oquirrh, and Wasatch fault zones. We used this curve rather than Keefer's (1984) distance-from-epicenter curve because of the reduced uncertainty associated with defining the extent of surface rup- ture as compared to predicting epicenter locations. Assuming that earthquakes occur on the end of the fault zone or segment nearest the Farmington Siding landslide complex, the relations shown in figure 22 and summarized in table 3 indicate that large earthquakes on any of these fault zones, except for the Levan and possibly Nephi segments of the Wasatch fault zone, could potentially induce lateral spread or flow failure at the landslide complex.

## Peak Ground Accelerations and Critical Accelerations

The ability of an earthquake to trigger liquefaction-induced landsliding at a given locality is controlled to a large degree by attenuation of the seismic energy. Although consideration of attenuation is implicit in the empirically derived curve in figure 22, a more rigorous analysis of the opportunity for liquefaction-induced landsliding at the Farmington Siding landslide complex relative to various earthquake source zones can be accomplished by determining the peak ground acceleration (PGA) using attenuation curves developed for north-central Utah by Campbell (1987). The PGA can also be determined for earthquakes of magnitude (M) 5, which are at the lower threshold of liquefaction-induced ground failure (Kuribayashi and Tatsuoka, 1975; Youd, 1977; Keefer, 1984) and are not constrained in location to mapped faults (Arabasz and others, 1992). The PGAs can then be compared to critical accelerations, the lowest values of peak ground acceleration required to induce liquefaction, at the Farmington Siding landslide complex. If the PGA associated with a given earthquake is less than the critical acceleration, the earthquake would be unlikely to trigger liquefaction-induced landsliding.

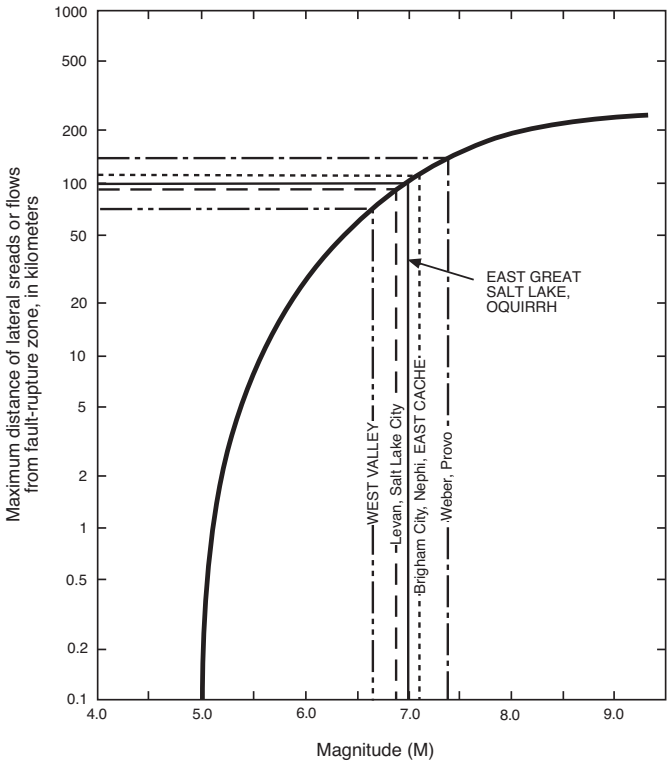


***Figure 22.*** *Empirically derived curve of maximum distance from fault-rupture zone to lateral spreads or flows (from Keefer, 1984), showing distances for maximum earthquakes on the East Cache, East Great Salt Lake, West Valley, and Oquirrh fault zones (upper case) and the six central Wasatch-fault-zone segments (lower case). Earthquake magnitudes from Keaton and others (1987), Youngs and others (1987), Machette and others (1991), Hecker (1993), Black and others (1995, 1996), and Olig and others (1996). Curve is based on reported surface-wave and moment magnitudes from 20 earthquakes worldwide.*

Anderson and others (1982) calculated critical accelerations at borehole sites across Davis County; table 1 summarizes their critical accelerations at sites within 1.6 kilometers (1 mi) of the Farmington Siding landslide complex. Anderson and others (1982) determined critical acceleration using the simplified procedure for calculating cyclic stress ratio (Seed and Idriss, 1971) in conjunction with an empirical method developed by Seed and others (1977) that relates standard penetration resistance of the soil with the cyclic stress ratio required to cause liquefaction. Critical accelerations were calculated for layers at least one foot thick consisting of sand, silty sand, or sandy silt with less than 15 percent clay and a plasticity index less than 5 (Anderson and others, 1982). Anderson and others (1982) assigned a representative critical acceleration for each site considering soil type, limitations of the SPT data, and consistencies within and between individual boreholes. As shown in table 1, critical accelerations range from 0.05 to 0.2 g at sites within and near the Farmington Siding landslide complex.

Table 4 summarizes PGA determinations for M 5 and maximum earthquakes on the fault zones and segments that could possibly trigger liquefaction induced landsliding at the Farmington Siding landslide complex as indicated in table 3. Again, we assume that the earthquakes occur on the end of the fault zone or segment nearest the landslide complex. As required by Campbell's (1987) attenuation curves, the distance parameter used in this analysis is distance from the center of the landslide complex to the nearest part of the seismogenic-rupture zone, as opposed to the surface-rupture zone in our analysis

***Table 3.***
*Opportunity for lateral spread or flow at the Farmington Siding landslide complex, based on empirical earthquake magnitude-distance relations.*

| FAULT ZONE/ Segment | $M_w$[1] | $R_{max}$[2](km) | $R_{SR}$ (km) | Earthquake Could Induce Landsliding At FSLC?[3] |
|---|---|---|---|---|
| EAST CACHE (central segment) | 7.1 | 110 | 75 | yes |
| EAST GREAT SALT LAKE | 7.0 | 100 | 25 | yes |
| WEST VALLEY | 6.7 | 70 | 20 | yes |
| OQUIRRH | 7.0 | 100 | 45 | yes |
| WASATCH: | | | | |
| Brigham City | 7.1 | 110 | 40 | yes |
| Weber | 7.4 | 130 | 2 | yes |
| Salt Lake City | 6.9 | 90 | 15 | yes |
| Provo | 7.4 | 130 | 55 | yes |
| Nephi | 7.1 | 110 | 110 | maybe |
| Levan | 6.9 | 90 | 190 | no |

[1]*Earthquake magnitudes from Keaton and others (1987), Youngs and others (1987), Machette and others (1991), Hecker (1993), McCalpin (1994), Black and others (1995, 1996), and Olig and others (1996).*

[2]*See figure 22.*

[3]*Earthquake could potentially trigger liquefaction-induced landsliding at the Farmington Siding landslide complex if* $R_{max} \geq R_{SR}$.

*Abbreviations:* $R_{max}$ *= maximum distance from surface rupture to induced lateral spread or flow;* $R_{SR}$ *= distance from middle of Farmington Siding landslide complex to nearest surface rupture on fault.*

using Keefer's (1984) curve. For the East Cache, West Valley, and most of the Wasatch fault zone, where the measured distances are approximately along the strike of the fault zones, the difference between distance to seismogenic rupture versus distance to surface rupture is negligible for the distances being considered. This is based on the assumptions that the fault zones are steeply dipping (Cook and Berg, 1961; Smith and Bruhn, 1984; Zoback, 1992) and that low-density (non-seismogenic) Cenozoic basin-fill sediments are less than 4 kilometers (2.5 mi) thick (Peterson and Oriel, 1970; Zoback, 1983; Mabey, 1992). Therefore, the distance values used to determine PGA for these fault zones are the same as the distance-to-surface-rupture ($R_{SR}$) values listed in table 3. For the west-dipping Weber segment of the Wasatch fault zone, which extends directly beneath the Farmington Siding landslide complex, we use a distance of 4 kilometers to determine PGA. For the west-dipping East Great Salt Lake and Oquirrh fault zones (Viveiros, 1986; Olig and others, 1996), which are southwest of the landslide complex, the distance values used to determine PGA are about 4 kilometers greater than the $R_{SR}$ values listed for these fault zones in table 3, based on an assumed 45-degree dip.

As summarized in table 4, earthquakes of M>5 (including maximum earthquakes) on the West Valley fault zone and Weber and Salt Lake City segments of the Wasatch fault zone, as well as maximum earthquakes on the East Great Salt Lake and Oquirrh fault zones and Brigham City and Provo segments of the Wasatch fault zone, could cause ground accelerations at the Farmington Siding landslide complex sufficient to trigger at least local liquefaction-induced ground failure. Widespread liquefaction-induced ground failure, which is possible when PGA exceeds the highest critical acceleration in the area (0.2 g) and would be most likely to result in large-scale landsliding, appears restricted to M>5 earthquakes on the Weber segment and maximum earthquakes on the Salt Lake City segment.

Based on the attenuation curves of Campbell (1987), a M 5 earthquake would theoretically need to be within a 20-kilometer (12-mi) radius of the Farmington Siding landslide complex to trigger local liquefaction-induced ground failure there. Empirical data, however, indicate the actual radius within which significant landslide movement is triggered by M 5 earthquakes may be much smaller, on the order of 5 kilometers (3 mi) or less (Keefer, 1984). Duration of shaking is a primary factor influencing liquefaction severity (Youd and Perkins, 1987), and lateral spreads and flows are more commonly triggered by the long-duration, low-frequency shaking characteristic of large earthquakes (Keefer, 1984). Given the apparent large ground displacements within the Farmington Siding landslide complex, such movement triggered by an earthquake as small as M 5 seems unlikely, unless perhaps the earthquake occurred directly beneath the landslide complex.

## Liquefaction Severity Index

The relative amounts of liquefaction-induced ground displacement triggered by earthquakes on various source zones can be compared by calculating the liquefaction severity index (LSI). The LSI was originally developed by Youd and Perkins (1987) to represent the maximum horizontal ground-failure displacement for lateral spreads in gently sloping Holocene fluvial deposits, which are among the materials that are especially susceptible to earthquake-induced landsliding (Keefer, 1984). The following LSI equation was subsequently developed (T.L. Youd and D.M. Perkins, personal communication, 1988,

***Table 4.***
*Opportunity for liquefaction-induced ground failure somewhere within the Farmington Siding landslide complex, based on peak ground acceleration and critical acceleration.*

| | M = 5.0 | | Maximum Earthquake[1] | |
|---|---|---|---|---|
| **FAULT ZONE/ Segment** | **PGA[2](g)** | **Liquefaction Opportunity[3]** | **PGA (g)** | **Liquefaction Opportunity** |
| EAST CACHE (central segment) | <0.02 | none | 0.04 | none |
| EAST GREAT SALT LAKE | 0.03 | none | 0.12 | moderate |
| WEST VALLEY | 0.05 | sufficient | 0.14 | moderate |
| OQUIRRH | <0.02 | none | 0.06 | sufficient |
| WASATCH: | | | | |
| Brigham City | 0.02 | none | 0.09 | sufficient |
| Weber | 0.23 | high | 0.54 | high |
| Salt Lake City | 0.07 | sufficient | 0.22 | high |
| Provo | <0.02 | none | 0.07 | sufficient |
| Nephi | <0.02 | none | 0.02 | none |

[1]*See table 3.*
[2]*Approximate peak ground acceleration at the Farmington Siding landslide complex based on attenuation curves of Campbell (1987).*
[3]*None (PGA <0.05 g); sufficient (PGA = 0.05 - 0.1 g); moderate (PGA = 0.1 - 0.2 g); high (PGA >0.2 g).*

in Mabey and Youd [1989]) to account for the regional variation of attenuation appropriate for Utah:

$$\log (LSI) = -3.53 - 1.60 \log (R) + 0.96 M_w \quad (1)$$

where LSI is the maximum ground displacement (inches), R is the distance (kilometers) to the nearest surface fault rupture, and $M_w$ is moment magnitude. LSI values can range from 0 to 100; Youd and Perkins (1987) considered displacements greater than 100 inches (2.5 m) to be so erratic and damaging that the corresponding LSI values would not be meaningful. Table 5 shows calculated LSIs for earthquakes on nearby source zones that could generate PGAs at the Farmington Siding landslide complex sufficient to trigger liquefaction-induced ground failure (see table 4). The LSI values range from 0.15 for a M 5 earthquake on the West Valley fault zone to greater than 100 for a $M_w$ 7.4 earthquake on the Weber segment of the Wasatch fault zone. These values support the idea that significant lateral displacements at the Farmington Siding landslide complex are most likely associated with large earthquakes on nearby fault segments, primarily the Weber segment of the Wasatch fault zone.

***Table 5.***
*Liquefaction severity index (LSI) at the Farmington Siding landslide complex.*

| FAULT ZONE/segment[1] | LSI (in) M=5.0 | LSI (in) Maximum Earthquake[2] |
|---|---|---|
| EAST GREAT SALT LAKE | - | 9.0 |
| WEST VALLEY | 0.15 | 6.6 |
| OQUIRRH | - | 3.5 |
| WASATCH: | | |
| Brigham City | - | 5.3 |
| Weber | 6.1 | >100 |
| Salt Lake City | 0.24 | 16.3 |
| Provo | - | 6.2 |

[1]*LSI was not calculated for earthquakes resulting in no liquefaction opportunity as noted in table 4.*
[2]*See table 3.*

## Estimated Newmark Landslide Displacements

The presence of scattered, relatively intact blocks of lacustrine sediment suggests that at least some flow failures within the Farmington Siding landslide complex may have initiated as coherent block slides that transformed into flows after some threshold amount of coseismic inertial displacement. The extensional style of deformation evident from the structural relations in trench FST2 also indicates that block sliding occurred at least locally. Initial movement of these landslides can be modeled under various earthquake scenarios using the sliding-block technique of Newmark (1965). If the model generates sufficient coseismic displacement of the intact landslide mass, then a tentative conclusion can be made that flow failures may have initiated as earthquake-triggered block slides. Thus, this analysis can also be used to compare the relative potential triggering effects of earthquakes from various source zones.

Newmark displacement can be estimated from the following empirical equation relating displacement, critical acceleration, and Arias intensity (Jibson, 1993; Jibson and Keefer, 1993):

$$\log D_N = 1.460 \log I_a - 6.642 a_c + 1.546 \quad (2)$$

where $D_N$ is Newmark displacement (centimeters), $I_a$ is Arias intensity (the integral over time of the square of the ground acceleration; Arias, 1970) (meters per second), and $a_c$ is critical acceleration (g). Arias intensity can be estimated from the following equation relating Arias intensity, earthquake magnitude, and source distance (Wilson and Keefer, 1985):

$$\log I_a = M_w - 2 \log R - 4.1 \quad (3)$$

where $I_a$ is in meters per second, $M_w$ is moment magnitude, and R is earthquake source distance (kilometers). Newmark displacements can therefore be estimated for given critical accelerations relative to earthquakes of various size at various distances from the Farmington Siding landslide complex.

Table 6 summarizes estimated Newmark displacements at sites with critical accelerations of 0.05 and 0.2 g, which is the range of critical accelerations in the vicinity of the Farmington Siding landslide complex (Anderson and others, 1982). Newmark displacements were estimated for maximum earthquakes on the fault zones and segments that could possibly trigger liquefaction-induced landsliding at the landslide complex as indicated in table 3. Values of earthquake source distance are based on the assumptions that the earthquakes occur on the end of the fault zone or segment nearest the landslide complex, that the earthquakes originate at a depth of 10 kilometers (6 mi) (Smith and Bruhn, 1984), and that the faults dip 45 degrees. The significance of the estimated Newmark displacements can be considered relative to a critical displacement that leads to general slope failure. A range of 5 to 10 centimeters (2-4 in) has been identified as representing critical displacements for various landslides in California and the Mississippi Valley (Wieczorek and others, 1985; Keefer and Wilson, 1989; Jibson and Keefer, 1993). Comparison of estimated Newmark displacements with this range of critical displacement indicates that coherent block slides which could evolve into flow failures could be triggered in areas of low critical acceleration (0.05 g) by maximum earthquakes on the East Great Salt Lake and West Valley fault zones, as well as the Brigham City, Weber, Salt Lake City, and Provo segments of the Wasatch fault zone. However, widespread earthquake-induced block sliding, which would be characterized by slope failure in areas of high (up to 0.2 g) as well as low critical accelerations, would likely only occur during a maximum earth-

***Table 6.***
*Estimated Newmark landslide displacements at the Farmington Siding landslide complex associated with maximum earthquakes.*

| FAULT ZONE/ Segment | $M_w$ | R (km) | $I_a$ (m/s) | $D_N$[1] (cm) | |
|---|---|---|---|---|---|
| | | | | $a_c$ = 0.05 g | $a_c$ = 0.2 g |
| EAST CACHE (central segment) | 7.1 | 76 | 0.17 | 1.23 | 0.12 |
| EAST GREAT SALT LAKE | 7.0 | 37 | 0.58 | 7.39 | 0.75 |
| WEST VALLEY | 6.7 | 24 | 0.69 | 9.52 | 0.96 |
| OQUIRRH | 7.0 | 56 | 0.25 | 2.16 | 0.22 |
| WASATCH: | | | | | |
| Brigham City | 7.1 | 42 | 0.57 | 7.20 | 0.73 |
| Weber | 7.4 | 13 | 11.81 | 600 | 60.7 |
| Salt Lake City | 6.9 | 21 | 1.43 | 27.6 | 2.78 |
| Provo | 7.4 | 57 | 0.61 | 7.95 | 0.80 |
| Nephi | 7.1 | 111 | 0.081 | 0.42 | 0.042 |

[1]*Newmark displacement; displacements are given for the range of critical accelerations (0.05 - 0.2 g) at selected sites in the vicinity of the Farmington Siding landslide complex as calculated by Anderson and others (1982).*
*Abbreviations: $M_w$ = moment magnitude; R = distance from earthquake source to center of Farmington Siding landslide complex; $I_a$ = Arias intensity; $a_c$ = critical acceleration.*

quake on the Weber segment.

Newmark displacement can also be used to evaluate the relative effects of smaller earthquakes with regard to block sliding. Of interest is the maximum source distance of an earthquake that could result in a critical displacement leading to general slope failure. Rearranging the terms in equation 2 allows calculation of Arias intensity from Newmark displacement and critical acceleration:

$$\log I_a = 0.685 (\log D_N + 6.642\, a_c - 1.546) \quad (4)$$

Likewise, rearranging the terms in equation 3 allows calculation of earthquake source distance from Arias intensity and moment magnitude:

$$\log R = 0.5 (M_w - \log I_a - 4.1) \quad (5)$$

To generate 5 centimeters (2 in) of Newmark displacement, equation 4 indicates that an Arias intensity of 0.44 meters per second would be required in areas with a critical acceleration of 0.05 g, and an Arias intensity of 3.03 meters per second would be required in areas with a critical acceleration of 0.2 g. Using these values and equation 5, we calculated earthquake source distances for earthquakes of $M_w$ 5.0, 6.0, and 6.5. As summarized in table 7, a $M_w$ 5.0 earthquake would need to originate directly beneath the Farmington Siding landslide complex, at or very near the top of the seismogenic crust, to produce 5 centimeters of coherent-block displacement in areas of low critical acceleration (0.05 g). A $M_w$ 5.0 earthquake could not produce 5 centimeters of coherent-block displacement in areas of high critical acceleration (0.2 g) because the earthquake source distance would be less than 4 kilometers, hence the earthquake would have to originate in non-seismogenic material. A $M_w$ 6.0 earthquake, which is believed to be about the threshold for surface fault rupture in Utah (Arabasz, 1984; Smith and Arabasz, 1991; Arabasz and others, 1992), would need to be on or in the immediate vicinity of the Weber segment of the Wasatch fault zone; a shallow earthquake (less than about 5 kilometers deep) would be necessary to produce 5 centimeters of coherent-block displacement in areas of high critical acceleration. A $M_w$ 6.5 earthquake would need to be on or near the Weber segment to produce 5 centimeters of coherent-block displacement in areas of high critical acceleration, but could be as far away as the near end of the Salt Lake City segment, and possibly the West Valley fault zone, to produce 5 centimeters of coherent-block displacement in areas of low critical acceleration.

***Table 7.***
*Maximum distance at which earthquake can generate 5 cm of Newmark displacement.*

| $a_c$ (g) | $M_w$ | R (km) |
|---|---|---|
| 0.05 | 5.0 | 4.2 |
| | 6.0 | 13.4 |
| | 6.5 | 23.9 |
| 0.2 | 5.0 | 1.6 |
| | 6.0 | 5.1 |
| | 6.5 | 9.1 |

*Abbreviations:*
*$a_c$ = critical acceleration;*
*$M_w$ = moment magnitude;*
*R = distance from earthquake source.*

## Fault-Zone Paleoseismicity

To further evaluate earthquakes as possible triggering mechanisms for landsliding at the Farmington Siding landslide complex, landslide timing can be compared to the paleoseismic histories of nearby earthquake source zones. Unfortunately, the timing of paleoseismic events on the East Great Salt Lake, Oquirrh, and West Valley fault zones remains unclear. The paleoseismic history of the East Great Salt Lake fault zone has not been studied, limiting radiocarbon ages of the Holocene-aged most recent event on the Oquirrh fault zone poorly constrain the timing of this event to a period spanning 3,100 years (Olig and others, 1996), and the six events on the West Valley fault zone during the past 13,000 years (Keaton and others, 1987) have not been dated. Also, paleoseismic histories in Utah are based on fault-trenching studies, which are subject to two inherent limitations. First, surface fault rupture in the Utah region only occurs in earthquakes with magnitudes greater than about 6.0-6.5 (Arabasz, 1984; Smith and Arabasz, 1991; Arabasz and others, 1992), whereas liquefaction-induced ground failure can be triggered by smaller earthquakes. Second, the oldest earthquake that can be documented in a fault study is determined by the depth to which a backhoe can dig. Reliable earthquake chronologies on the Wasatch fault zone typically are limited to about the last 6,000 years. However, despite the lack of a clear record of the timing of some possible earthquakes that might have generated liquefaction-induced ground failure, the timing of the largest earthquakes (and therefore the most likely earthquakes to trigger landsliding) on the well-studied Wasatch fault zone can still provide insight into its possible role in landsliding at the Farmington Siding landslide complex.

Numerous fault studies have been completed that constrain the timing of past surface-faulting earthquakes on the Brigham City, Weber, Salt Lake City, and Provo segments of the Wasatch fault zone (Machette and others, 1987; Schwartz and others, 1988; Personius, 1990; Forman and others, 1991; Lund and others, 1991; McCalpin and Forman, 1994; McCalpin and others, 1994; Black and others, 1995, 1996). As shown in figure 23, comparison of the results of these studies with the timing of Farmington Siding landslide events indicates a close correspondence between landsliding and certain earthquakes. Within uncertainty limits, earthquakes on the Brigham City segment coincide with all four possible landslide events, and earthquakes on the Weber segment occurred around the times of the third(?) and fourth (most recent) landslide events. Earthquakes also occurred on the Salt Lake City and Provo segments around the time of the fourth landslide event. The earthquake chronologies generally do not extend beyond 6,000 years ago, so the possibility exists that unrecognized and/or undated older earthquakes may also correspond to the earlier landslide events. Of particular significance is evidence provided by geometric reconstructions and slip-rate estimates for two or three early Holocene to latest Pleistocene earthquakes on the Weber segment (McCalpin and others, 1994). Given the high potential for large Weber-segment earthquakes to trigger liquefaction-induced landsliding at the Farmington Siding landslide complex, an association between these earthquakes and landslide events seems likely. Furthermore, the landslide timing therefore appears to provide indirect evidence for the approximate timing of these Weber-segment earthquakes that predate the late Holocene events documented in paleoseismic trenching studies (Hylland, 1996).

Figure 23 shows a likely correspondence between apparent earthquake-triggered landslides and lacustral highstands approximately at or above the historical high of 1,284 meters (4,212 ft). At the same time, numerous large earthquakes have occurred on the central segments of the Wasatch fault zone that apparently do not coincide with Farmington Siding landslide events, including the most recent earthquake on the nearby Weber segment which occurred after the most recent major landslide. Either geologic and hydrologic conditions at the time of these earthquakes were such that little or no slope move-

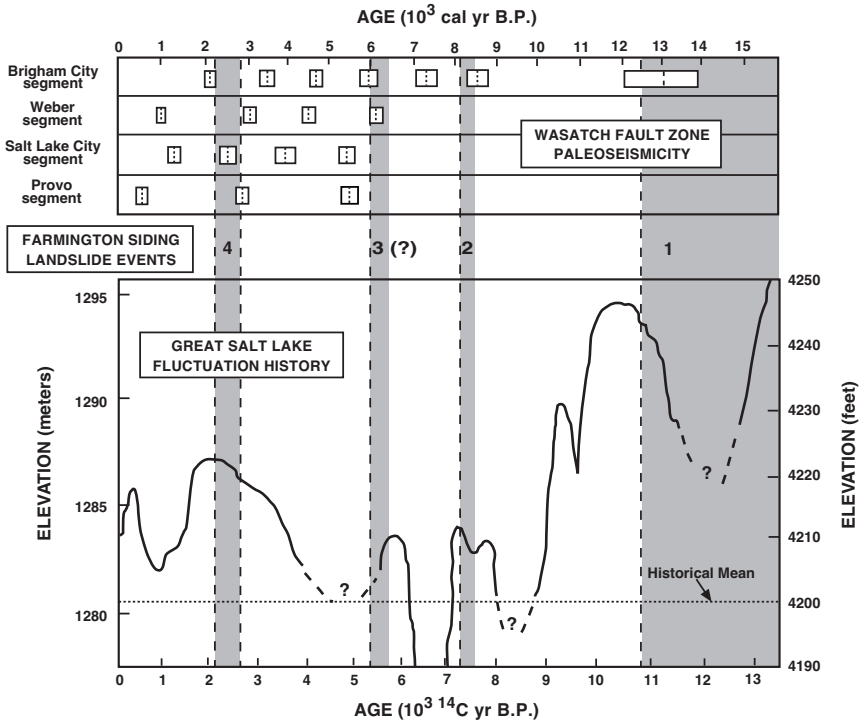


***Figure 23.*** *Comparison of the timing of landslide events (shaded areas) at the Farmington Siding landslide complex with Wasatch-fault-zone paleoseismicity (top) and Great Salt Lake fluctuations (bottom). Earthquake chronologies from McCalpin and Nishenko (1996). Reliable pre-6,000 yr B.P. earthquake chronologies for the Weber, Salt Lake City, and Provo segments are not available. Great Salt Lake hydrograph after Murchison (1989). Shaded area for landslide event 1 represents period between the Provo Stage of the Bonneville paleolake cycle and the Gilbert highstand of Great Salt Lake. Shaded areas for landslide events 2 through 4 represent 2σ limits of radiocarbon ages discussed in text. Dashed lines represent limiting ages.*

ment occurred, or evidence for landsliding has not yet been observed. Some ground disturbance associated with minor landsliding seems likely to have occurred during at least some of these earthquakes, especially those on the nearby Weber segment.

## HAZARD POTENTIAL

The results of this study indicate a correspondence between large earthquakes on the Wasatch fault zone, high lacustral and associated ground-water levels, and liquefaction-induced landsliding. Comparison of the average recurrence intervals of large earthquakes on the Brigham City, Weber, and Salt Lake City fault segments with the elapsed time since the most recent events (see figure 23) indicates that the chance of a large earthquake on one of these segments in the near future cannot be discounted (McCalpin and Nishenko, 1996). Under certain circumstances, large earthquakes on other nearby fault zones as well as moderate "random" earthquakes may also have the potential to trigger liquefaction-induced landsliding at the Farmington Siding landslide complex.

The susceptibility to liquefaction-induced landsliding in the vicinity of the Farmington Siding landslide complex may presently be less than at other times during the Holocene, given the lower average lake and associated ground-water levels during historical time as compared to those that characterized much of the Holocene. Under modern long-term climatic conditions, however, an episode of three to five years of above-average precipitation that could cause an abrupt lake-level rise can be expected on average about once every 100-110 years (Karl and Young, 1986). In historical time, Great Salt Lake has risen as much as about 3 meters (12 ft) above its mean level to reach an elevation of 1,284 meters (4,212 ft), once in 1873 and again in 1986-1987 (Currey, 1987, 1990); the lake could rise to an elevation of 1,285 meters (4,215 ft) during a more prolonged episode of increased precipitation (Atwood and Mabey, 1995). Also, the stratified nature of the sediments in the vicinity of the landslide complex can result in shallow, locally "perched" ground water, especially during and following periods of intense or prolonged precipitation or snowmelt. Therefore, a relatively high potential for liquefaction-induced landsliding would exist if the area experienced strong ground shaking during a time when lake levels were near or above the historical high, or when local ground-water levels were increased as the result of abnormally high seasonal precipitation or snowmelt.

Anderson and others (1982) mapped the Farmington Siding landslide complex and adjacent flank areas to the northwest and southeast as a high-liquefaction-potential zone, based on a greater-than-50 percent probability of critical accelerations being exceeded sometime within a 100-year period, with ground water at depths of less than 3 meters (10 ft). Anderson and others (1982) concluded that, based on ground slope, the most likely modes of liquefaction-induced ground failure in these areas would be loss of bearing capacity and lateral spread. As indicated by the LSI values in table 5, ground displacements associated with future lateral spread at the landslide complex could vary considerably depending on earthquake magnitude and proximity. The LSI values can be compared to the ranges given in table 8 to determine relative levels of expected damage to structures as summarized by Youd (1980).

***Table 8***.

*Relationships between ground displacement and damage to structures (from Youd, 1980).*

| Ground Displacement | Level Of Expected Damage |
|---|---|
| Less than 4 inches | Little damage, repairable |
| 4 to 12 inches | Severe damage, repairable |
| 12 to 24 inches | Severe damage, non-repairable |
| More than 24 inches | Collapse, non-repairable |

Anderson and others (1982) mapped the crown area east and northeast of the Farmington Siding landslide complex as a moderate-liquefaction-potential zone, based on a 10 to 50 percent probability of critical accelerations being exceeded sometime within a 100-year period, with ground water at depths of less than 9 meters (30 ft). Anderson and others (1982) concluded that, based on ground slope, the most likely mode of liquefaction-induced ground failure in this area would be flow failure. The amount of ground displacement associated with flow failure is difficult to quantify. However, flow failure is the most catastrophic mode of liquefaction-induced ground failure (Tinsley and others, 1985), and therefore can cause the most severe damage to structures. Flow failures commonly displace soil masses tens of meters, and under favorable circumstances can displace material tens of kilometers at velocities of tens of kilometers an hour (Tinsley and others, 1985). Rapid flows are among the predominant landslide-related threats to life, and along with lateral spreads are among the leading causes of property damage from earthquake-induced landslides (Keefer, 1984).

Harty and others (1993) concluded that the relative potential for future liquefaction-induced landsliding at the Farmington Siding landslide complex is higher in the northern part of the complex than in the southern part. The results of this study support their conclusion, as the sequence of major landslide events appears to have generally progressed from south to north. Various features indicate late Holocene stability of the southern part of the complex, but not of the northern part. Thus, the relative hazard associated with future liquefaction-induced landsliding appears to be higher in the northern part of the complex than in the southern part. Likewise, the relative hazard associated with future liquefaction-induced landsliding in the unfailed crown area adjacent to the north

and northeast margins of the complex appears to be higher than in the unfailed flank and crown areas adjacent to the northwest, east, and southeast margins of the complex. This is because the existing landslide scarp appears to have resulted from headward (northeastward) migration in the former area, but not in the latter areas, during the most recent landslide event.

## CONCLUSIONS AND RECOMMENDATIONS

The Farmington Siding landslide complex is a large area of liquefaction-induced landslides showing evidence of recurrent movement during latest Pleistocene and Holocene time. Based on geotechnical borehole data, liquefaction appears to have occurred in loose offshore-lacustrine deposits that overlie relatively dense transgressional-lacustrine or alluvial deposits. Geologic evidence for liquefaction within the complex includes injected sand, attenuation and disruption of silt and clay interbeds within sand beds, and failure of very gentle slopes not otherwise susceptible to landsliding. Lateral spread and flow have both been important slope-failure modes, but flow has had a dominant influence on the morphology of the complex. Rotational or translational block sliding may have played a significant role at least locally in scarp formation. Hummocks within the complex may have been displaced laterally as much as a kilometer or more during one or more landsliding events. Landslide deformation within the hummocks is characterized by extensional high-angle faults with apparent displacements ranging from a few centimeters to 2 meters (7 ft). Strong folding and low-angle faulting within the hummocks probably represent penecontemporaneous deformation of sediments beneath Lake Bonneville that predates subaerial landsliding.

Relative and absolute timing information indicates at least three, and possibly four, landslide events: the first sometime between 14,500 and 10,900 $^{14}$C yr B.P.; the second just prior to 7,310 ± 60 $^{14}$C yr B.P. (8,100 [+250, -200] cal yr B.P.); the third(?) sometime prior to 5,280 ± 60 $^{14}$C yr B.P. (6,000 [+300, -250] cal yr B.P.); and the fourth between 2,340 ± 60 and 2,440 ± 70 $^{14}$C yr B.P. (2,750 and 2,150 cal yr B.P.). The landslide events generally progressed from south to north, and the southern part of the complex has remained relatively stable during the late Holocene. The present main scarp in the northeastern part of the complex formed as the result of probable headward migration during the most recent landslide event, whereas the pre-existing scarp in the northwestern part of the complex acted as a lateral scarp during this event and was only slightly modified. The timing of these landslide events corresponds well with the timing of Great Salt Lake highstands near or above the historical high, and associated high ground-water levels.

Empirical earthquake magnitude-distance relations indicate that liquefaction-induced landsliding at the Farmington Siding landslide complex could have been triggered by large earthquakes on the East Cache, East Great Salt Lake, West Valley, and Oquirrh fault zones, as well as the Brigham City, Weber, Salt Lake City, Provo, and possibly Nephi segments of the Wasatch fault zone. However, comparison of expected PGAs with calculated critical accelerations, as well as quantitative estimates of LSI and Newmark landslide displacements, confirm that the most likely earthquakes to trigger significant liquefaction-induced landsliding at the Farmington Siding landslide complex are large earthquakes on the nearby Weber segment. The high liquefaction opportunity and potential for long-duration strong ground shaking associated with large Weber-segment earthquakes results in a relatively higher potential for significant liquefaction-induced landsliding.

The timing of the three earliest Farmington Siding landslide events corresponds well with documented earthquakes on the Brigham City segment of the Wasatch fault zone, and may correspond with earthquakes on other nearby segments for which chronologies do not extend back far enough to include those events. These landslide events likely were associated with suspected, but as yet undated, earthquakes on the Weber segment. The fourth landslide event occurred around the time of large earthquakes on the Brigham City, Weber, Salt Lake City, and Provo segments. Other large earthquakes on these fault segments apparently have occurred that did not trigger landsliding at the Farmington Siding landslide complex, at least not of sufficient magnitude to cause major ground disturbance and to have been recognized in this and previous studies. In addition to an association with earthquakes, landslide timing also corresponds well with Great Salt Lake highstands. Therefore, relatively major landsliding appears to be associated with large earthquakes coincident with high lake and ground-water levels.

The susceptibility to liquefaction-induced landsliding in the vicinity of the Farmington Siding landslide complex may presently be less than at other times during the Holocene, given the lower average lake and associated ground-water levels during historical time as compared to those that characterized much of the Holocene. However, a higher potential for liquefaction-induced landsliding would exist if the area experienced strong ground shaking during a time of increased soil pore-water pressures associated with abnormally high lake and/or ground-water levels. Based on geologic conditions and the pattern of previous landsliding, the relative hazard associated with liquefaction-induced landsliding is higher in the northern part of the landslide complex and in the crown area adjacent to the north and northeast margins of the complex, and is lower in the southern part of the complex and in the flank and crown areas adjacent to the northwest, east, and southeast margins of the complex. Given the relative likelihood of a large earthquake in this part of Utah in the near future and the possible consequences of large-displacement slope failure involving lateral spread or flow, special consideration of the potential for liquefaction-induced landsliding in the northern part of the complex and in the crown area north and northeast of the complex is warranted in land-use planning.

To ensure safe and responsible development in the vicinity of the Farmington Siding landslide complex, particularly in the northern part of the complex and in the crown area north and northeast of the complex, we recommend that site-specific geotechnical-engineering and engineering-geologic studies be completed within a framework of area-wide land-use planning. Although this study addresses various geologic aspects of the relative hazard associated with liquefaction-induced landsliding, it is not a substitute for site-specific hazard evaluations.

Lowe (1990, 1993) provides recommendations for land-use planning in liquefaction-hazard areas and scope of site-specific liquefaction evaluations in Davis County, and Keaton and Jalbert (1991) present a useful method for analyzing liquefaction-induced ground-failure hazard. Site-specific studies must go beyond evaluating liquefaction susceptibility; they need to determine the potential for liquefaction-induced ground failure relative to an appropriate level of earthquake ground acceleration (for example, a probabilistic acceleration associated with a given exposure time as shown on maps by Youngs and others [1987], Algermissen and others [1990], or Frankel and others [1996]). If the analysis indicates ground failure can be expected, then the amount of ground displacement should be estimated. Bartlett and Youd (1992) have developed a comprehensive empirical model that can be used to determine ground displacement based on site-specific factors, including: earthquake magnitude; distance to seismic source; ground slope or free-face ratio; and thickness, fines content, and average grain size of liquefiable soils. This and other techniques for estimating liquefaction-induced ground displacement are summarized in Glaser (1994). Finally, the site-specific study should evaluate the consequences of ground failure and recommend appropriate hazard-reduction measures. As stated in Keaton and Jalbert (1991), this involves consideration of the site conditions, type of development, probability of earthquake ground accelerations large enough to induce liquefaction, and likely mode of ground failure.

In general, the liquefaction hazard can be reduced on a site-specific scale through a variety of engineering techniques, such as special foundation design, removal and replacement of material susceptible to liquefaction, soil densification, grouting or chemical stabilization, loading or buttressing, and dewatering through the use of wells, drains, or other ground-water controls (National Research Council, 1985). Any of these techniques, however, could be relatively ineffective in reducing the ground-displacement hazard if applied only locally within a large area of potential landsliding. Therefore, the hazard associated with the Farmington Siding landslide complex can probably best be reduced by addressing the issue on an area-wide scale. The hazard can be reduced administratively by simply avoiding development in areas with a relatively higher potential for liquefaction-induced landsliding. This option, however, is often impractical in rapidly growing areas with limited vacant land, and is not a consideration in previously developed areas. Kockelman (1986) lists other administrative alternatives that can be considered to reduce the hazards associated with landsliding. The final decisions regarding development on and in the vicinity of the Farmington Siding landslide complex should be based on careful consideration of the nature of past landsliding, liquefaction potential, seismic risk, and sound land-use planning practices involving conscious decisions to define levels of acceptable risk.

## ACKNOWLEDGMENTS

This research was sponsored jointly by the Utah Geological Survey and U.S. Geological Survey, National Earthquake Hazards Reduction Program (award no. 1434-94-G-2498). We appreciate the cooperation and assistance of Davis County and the city of Farmington. Frank Ashland, Charlie Bishop, Bill Black, Dar Day, Janine Jarva, Bea Mayes, Noah Snyder, and Brad and Rob Squires provided assistance in the field. Backhoe services were provided by Ken Hardy's Backhoe Work of Farmington, Utah, and the city of Farmington. Les Youd (Brigham Young University) and Jeff Keaton (AGRA Earth & Environmental, Inc.) visited the trench sites, as did Gary Christenson (UGS), who also provided insight and guidance during the course of this project and critically reviewed the manuscript. Figures were drafted by Bea Mayes, Jim Parker, Vicky Clarke, and Sharon Hamre (UGS). We appreciate helpful reviews of the manuscript by Kimm Harty (UGS) and David Keefer, Randy Jibson, and Steve Obermeier (USGS). Finally, we thank the people of Farmington who granted access for trenching on their property, including Rodney Hess, Merlin Morrison, Candland Olsen, Aaron Richards, Milton Sessions, and the Oakridge Country Club.

# REFERENCES


Algermissen, S.T., Perkins, D.M., Thenhaus, P.C., Hanson, S.L., and Bender, B.L., 1990, Probabilistic earthquake acceleration and velocity maps for the United States and Puerto Rico: U.S. Geological Survey Miscellaneous Field Studies Map MF-2120, scale 1:7,500,000.

Anderson, L.R., Keaton, J.R., Aubrey, Kevin, and Ellis, S.J., 1982, Liquefaction potential map for Davis County, Utah: Logan, Utah State University Department of Civil and Environmental Engineering and Dames & Moore Consulting Engineers, Final Technical Report for the U.S. Geological Survey, 50 p. (published as Utah Geological Survey Contract Report 94-7).

Arabasz, W.J., 1984, Earthquake behavior in the Wasatch Front area - Association with geologic structure, space-time occurrence, and stress state, *in* Hays, W.W., and Gori, P.L., editors, Proceedings of Conference XXVI - A workshop on evaluation of regional and urban earthquake hazards and risk in Utah: U.S. Geological Survey Open-File Report 84-763, p. 310-339.

Arabasz, W.J., Pechmann, J.C., and Brown, E.D., 1992, Observational seismology and the evaluation of earthquake hazards and risk in the Wasatch Front area, Utah, *in* Gori, P.L., and Hays, W.W., editors, Assessment of regional earthquake hazards and risk along the Wasatch Front, Utah: U.S. Geological Survey Professional Paper 1500-A-J, p. D1-D36.

Arias, A., 1970, A measure of earthquake intensity, *in* Hansen, R.J., editor, Seismic design for nuclear power plants: Cambridge, Massachusetts Institute of Technology Press, p. 438-483.

Atwood, Genevieve, and Mabey, D.R., 1995, Flooding hazards associated with Great Salt Lake, *in* Lund, W.R., editor, Environmental and engineering geology of the Wasatch Front region: Utah Geological Association Publication 24, p. 483-493.

Bartlett, S.F., and Youd, T.L., 1992, Empirical analysis of horizontal ground displacement generated by liquefaction-induced lateral spreads: National Center for Earthquake Engineering Research Technical Report NCEER-92-0021, 63 p.

Birkeland, P.W., Machette, M.N., and Haller, K.M., 1991, Soils as a tool for applied Quaternary geology: Utah Geological and Mineral Survey Miscellaneous Publication 91-3, 63 p.

Black, B.D., Lund, W.R., and Mayes, B.H., 1995, Large earthquakes on the Salt Lake City segment of the Wasatch fault zone - Summary of new information from the South Fork Dry Creek site, Salt Lake County, Utah, *in* Lund, W.R., editor, Environmental and engineering geology of the Wasatch Front region: Utah Geological Association Publication 24, p. 11-30.

Black, B.D., Lund, W.R., Schwartz, D.P., Gill, H.E., and Mayes, B.H., 1996, Paleoseismic investigation on the Salt Lake City segment of the Wasatch fault zone at the South Fork Dry Creek and Dry Gulch sites, Salt Lake County, Utah, *in* Lund, W.R., editor, Paleoseismology of Utah, Volume 7: Utah Geological Survey Special Study 92, 22 p.

Campbell, K.W., 1987, Predicting strong ground motion in Utah, *in* Gori, P.L., and Hays, W.W., editors, Assessment of regional earthquake hazards and risk along the Wasatch Front, Utah: U.S. Geological Survey Open-File Report 87-585, p. L1-L90.

Chen and Associates, 1988, Geotechnical investigation, Davis County Criminal Justice Complex, Clark Lane and 650 West, Farmington, Utah: Salt Lake City, Utah, unpublished consultant's report for Edwards and Daniels Associates, Architects, 17 p.

Cook, K.L., and Berg, J.W., Jr., 1961, Regional gravity survey along the central and southern Wasatch Front, Utah: U.S. Geological Survey Professional Paper 316-E, p. 75-89.

Currey, D.R., 1980, Coastal geomorphology of Great Salt Lake and vicinity, *in* Gwynn, J.W., editor, Great Salt Lake - A scientific, historical and economic overview: Utah Geological and Mineral Survey Bulletin 116, p. 69-82.

— 1987, Great Salt Lake levels - Holocene geomorphic development and hydrographic history, in Laboratory for terrestrial physics: Greenbelt, Maryland, NASA Goddard Space Flight Center, 3rd Annual Landsat Workshop, p. 127-132.

— 1990, Quaternary paleolakes in the evolution of semidesert basins, with special emphasis on Lake Bonneville and the Great Basin, U.S.A.: Palaeogeography, Palaeoclimatology, Palaeoecology, v. 76, p. 189-214.

Currey, D.R., Berry, M.S., Douglass, G.E., Merola, J.A., Murchison, S.B., and Ridd, M.K., 1988, The highest Holocene stage of Great Salt Lake, Utah [abs.]: Geological Society of America Abstracts with Programs, v. 20, no. 6, p. 411.

Currey, D.R., and James, S.R., 1982, Paleoenvironments of the northeastern Great Basin and northeastern Basin rim region - A review of geological and biological evidence, *in* Madsen, D.B., and O'Connell, J.F., editors, Man and environment in the Great Basin: Society for American Archaeology, SAA Papers No. 2, p. 27-52.

Currey, D.R., and Oviatt, C.G., 1985, Durations, average rates, and probable causes of Lake Bonneville expansions, still-stands, and contractions during the last deep-lake cycle, 32,000 to 10,000 years ago, *in* Kay, P.A., and Diaz, H.F., editors, Problems of and prospects for predicting Great Salt Lake levels - Proceedings of a NOAA Conference, March 26-28, 1985: Salt Lake City, University of Utah, Center for Public Affairs and Administration, p. 9-24.

Currey, D.R., Oviatt, C.G., and Plyler, G.B., 1983, Lake Bonneville stratigraphy, geomorphology, and isostatic deformation in west-central Utah, *in* Gurgel, K.D., editor, Geologic excursions in neotectonics and engineering geology in Utah, Geological Society of America Guidebook - Part IV: Utah Geological and Mineral Survey Special Study 62, p. 63-82.

Eardley, A.J., 1962, Glauber's salt bed west of Promontory Point, Great Salt Lake: Utah Geological and Mineral Survey Special Study No. 1, 12 p.

Erickson, A.J., and Wilson, Lemoyne, 1968, Soil survey of Davis-Weber area, Utah: U.S. Department of Agriculture, Soil Conservation Service, in cooperation with Utah Agricultural Experiment Station, 149 p.

Everitt, Ben, 1991, Stratigraphy of eastern Farmington Bay: Utah Geological and Mineral Survey, Survey Notes, v. 24, no. 3, p. 27-29.

Forman, S.L., Nelson, A.R., and McCalpin, J.P., 1991, Thermoluminescence dating of fault-scarp-derived colluvium - Deciphering the timing of paleoearthquakes on the Weber segment of the Wasatch fault zone, north central Utah: Journal of Geophysical Research, v. 96, no. B1, p. 595-605.

Frankel, Arthur, Mueller, Charles, Barnhard, Theodore, Perkins, David, Leyendecker, E.V., Dickman, Nancy, Hanson, Stanley, and Hopper, Margaret, 1996, National seismic-hazard maps - Documentation, June 1996: U.S. Geological Survey, Open-File Report 96-532, 110 p.

Gile, L.H., Peterson, F.F., and Grossman, R.B., 1966, Morphological

and genetic sequences of carbonate accumulation in desert soils: Soil Science, v. 101, no. 5, p. 347-360.

Glaser, S.D., 1994, Estimation of surface displacements due to earthquake excitation of saturated sands: Earthquake Spectra, v. 10, no. 3, p. 289-517.

Green, S.A., and Currey, D.R., 1988, The Stansbury shoreline and other transgressive deposits of the Bonneville lake cycle, *in* Machette, M.N., editor, In the footsteps of G.K. Gilbert - Lake Bonneville and neotectonics of the eastern Basin and Range Province, Geological Society of America Guidebook for Field Trip Twelve: Utah Geological and Mineral Survey Miscellaneous Publication 88-1, p. 55-57.

Guthrie, R.L., and Witty, J.E., 1982, New designations for soil horizons and layers and the new Soil Survey Manual: Soil Science of America Journal, v. 46, p. 443-444.

Harty, K.M., Lowe, Mike, and Christenson, G.E., 1993, Hazard potential and paleoseismic implications of liquefaction-induced landslides along the Wasatch Front, Utah: Utah Geological Survey, unpublished Final Technical Report for the U.S. Geological Survey, 57 p.

Hecker, Suzanne, 1993, Quaternary tectonics of Utah with emphasis on earthquake-hazard characterization: Utah Geological Survey Bulletin 127, 157 p.

Hylland, M.D., 1996, Paleoseismic analysis of the liquefaction-induced Farmington Siding landslide complex, Wasatch Front, Utah [abs.]: Geological Society of America Abstracts with Programs, v. 28, no. 7, p. A-157.

Hylland, M.D., and Lowe, Mike, 1995, Hazard potential, failure type, and timing of liquefaction-induced landsliding in the Farmington Siding landslide complex, Wasatch Front, Utah: Utah Geological Survey Open-File Report 332, 47 p.

Jibson, R.W., 1993, Predicting earthquake-induced landslide displacements using Newmark's sliding block analysis: National Research Council, Transportation Research Record 1411, p. 9-17.

Jibson, R.W., and Keefer, D.K., 1993, Analysis of the seismic origin of landslides - Examples from the New Madrid seismic zone: Geological Society of America Bulletin, v. 105, p. 521-536.

Kanamori, Hiroo, 1983, Magnitude scale and quantification of earthquakes: Tectonophysics, v. 93, p. 185-199.

Karl, T.R., and Young, P.J., 1986, Recent heavy precipitation in the vicinity of Great Salt Lake - Just how unusual?: Journal of Climate and Applied Meteorology, v. 25, p. 353-363.

Keaton, J.R., Currey, D.R., and Olig, S.S., 1987, Paleoseismicity and earthquake hazards evaluation of the West Valley fault zone, Salt Lake City urban area, Utah: Salt Lake City, Dames & Moore and University of Utah Department of Geography, Final Technical Report for the U.S. Geological Survey, 55 p. (published as Utah Geological Survey Contract Report 93-8).

Keaton, J.R., and Jalbert, L.A., 1991, Systematic liquefaction-induced ground failure hazard analysis, *in* McCalpin, James, editor, Proceedings of the 27th Symposium on Engineering Geology and Geotechnical Engineering, April 1991: Logan, Utah State University, p. 24-1 - 24-13.

Keefer, D.K., 1984, Landslides caused by earthquakes: Geological Society of America Bulletin, v. 95, p. 406-421.

Keefer, D.K., and Wilson, R.C., 1989, Predicting earthquake-induced landslides, with emphasis on arid and semi-arid environments, *in* Sadler, P.M., and Morton, D.M., editors, Landslides in a semi-arid environment: Riverside, California, Inland Geological Society, v. 2, p. 118-149.

Kockelman, W.J., 1986, Some techniques for reducing landslide hazards: Bulletin of the Association of Engineering Geologists, v. XXIII, no. 1, p. 29-52.

Kuribayashi, Eiichi, and Tatsuoka, Fumio, 1975, Brief review of liquefaction during earthquakes in Japan: Soils and Foundations, v. 15, no. 4, p. 81-92.

Lowe, Mike, editor, 1990, Geologic hazards and land-use planning - Background, explanation, and guidelines for development in Davis County in designated geologic hazards special study areas: Utah Geological and Mineral Survey Open-File Report 198, 73 p.

— 1993, Liquefaction hazards - A guide for land-use planning, Davis County, Utah, *in* Gori, P.L., editor, Applications of research from the U.S. Geological Survey program, assessment of regional earthquake hazards and risk along the Wasatch Front, Utah: U.S. Geological Survey Professional Paper 1519, p. 151-157.

Lowe, Mike, and Harty, K.M., 1993, Geomorphology and failure history of the earthquake-induced Farmington Siding landslide complex, Davis County, Utah [abs.]: Geological Society of America Abstracts with Programs, v. 25, no. 5, p. 111.

Lowe, Mike, Harty, K.M., and Hylland, M.D., 1995, Geomorphology and failure history of the earthquake-induced Farmington Siding landslide complex, Davis County, Utah, *in* Lund, W.R., editor, Environmental and engineering geology of the Wasatch Front region: Utah Geological Association Publication 24, p. 205-219.

Lund, W.R., Schwartz, D.P., Mulvey, W.E., Budding, K.E., and Black, B.D., 1991, Fault behavior and earthquake recurrence on the Provo segment of the Wasatch fault zone at Mapleton, Utah County, Utah, in Lund, W.R., editor, Paleoseismology of Utah, Volume 1: Utah Geological and Mineral Survey Special Study 75, 41 p.

Mabey, D.R., 1992, Subsurface geology along the Wasatch Front, *in* Gori, P.L., and Hays, W.W., editors, Assessment of regional earthquake hazards and risk along the Wasatch Front, Utah: U.S. Geological Survey Professional Paper 1500-A-J, p. C1-C16.

Mabey, M.A., and Youd, T.L., 1989, Liquefaction severity index maps of the state of Utah, *in* Watters, R.J., editor, Engineering geology and geotechnical engineering: Rotterdam, A.A. Balkema, Proceedings of the 25th Annual Engineering Geology and Geotechnical Engineering Symposium, Reno, Nevada, p. 305-312.

Machette, M.N., 1985, Calcic soils of the southwestern United States, *in* Weide, D.L., editor, Soils and Quaternary geology of the southwestern United States: Geological Society of America Special Paper 203, p. 1-21.

Machette, M.N., Personius, S.F., and Nelson, A.R., 1987, Quaternary geology along the Wasatch fault zone - Segmentation, recent investigations, and preliminary conclusions, *in* Gori, P.L., and Hays, W.W., editors, Assessment of regional earthquake hazards and risk along the Wasatch Front, Utah: U.S. Geological Survey Open-File Report 87-585, p. A1-A72.

— 1992, Paleoseismology of the Wasatch fault zone - A summary of recent investigations, interpretations, and conclusions, *in* Gori, P.L., and Hays, W.W., editors, Assessment of regional earthquake hazards and risk along the Wasatch Front, Utah: U.S. Geological Survey Professional Paper 1500-A-J, p. A1-A71.

Machette, M.N., Personius, S.F., Nelson, A.R., Schwartz, D.P., and Lund, W.R., 1991, The Wasatch fault zone, Utah - Segmentation and history of Holocene earthquakes: Journal of Structural Geology, v. 13, no. 2, p. 137-149.

Madsen, D.B., and Currey, D.R., 1979, Late Quaternary glacial and vegetation changes, Little Cottonwood Canyon area, Wasatch Mountains, Utah: Quaternary Research, v. 12, p. 254-270.

McCalpin, J.P., 1994, Neotectonic deformation along the East Cache fault zone, Cache County, Utah, *in* Lund, W.R., editor, Paleoseismology of Utah, Volume 5: Utah Geological Survey Special Study 83, 37 p.

McCalpin, James, and Forman, S.L., 1994, Assessing the paleoseismic activity of the Brigham City segment, Wasatch fault zone, Utah - Site of the next major earthquake on the Wasatch Front?: Utah State University and Byrd Polar Research Institute, unpublished Final Technical Report for the U.S. Geological Survey, 19 p.

McCalpin, J.P., Forman, S.L., and Lowe, Mike, 1994, Reevaluation of Holocene faulting at the Kaysville site, Weber segment of the Wasatch fault zone, Utah: Tectonics, v. 13, no. 1, p. 1-16.

McCalpin, J.P., and Nishenko, S.P., 1996, Holocene paleoseismicity, temporal clustering, and probabilities of future large (M>7) earthquakes on the Wasatch fault zone, Utah: Journal of Geophysical Research, v. 101, no. B3, p. 6233-6253.

McCoy, W.D., 1987, Quaternary aminostratigraphy of the Bonneville basin, western United States: Geological Society of America Bulletin, v. 98, p. 99-112.

Miller, R.D., 1980, Surficial geologic map along part of the Wasatch Front, Salt Lake valley, Utah: U.S. Geological Survey Miscellaneous Field Studies Map MF-1198, scale 1:100,000.

Miller, R.D., Olsen, H.W., Erickson, G.S., Miller, C.H., and Odum, J.K., 1981, Basic data report of selected samples collected from six test holes at five sites in the Great Salt Lake and Utah Lake valleys, Utah: U.S. Geological Survey Open-File Report 81-179, 49 p.

Murchison, S.B., 1989, Fluctuation history of Great Salt Lake, Utah, during the last 13,000 years: Salt Lake City, University of Utah, Ph.D. thesis, 137 p.

National Research Council, 1985, Liquefaction of soils during earthquakes: Washington, D.C., National Academy Press, 240 p.

Nelson, A.R., and Personius, S.F., 1993, Surficial geologic map of the Weber segment, Wasatch fault zone, Weber and Davis Counties, Utah: U.S. Geological Survey Miscellaneous Investigations Series Map I-2199, 22 p. pamphlet, scale 1:50,000.

Newmark, N.M., 1965, Effects of earthquakes on dams and embankments: Geotechnique, v. 15, p. 139-160.

Obermeier, Stephen, 1987, Identification and geologic characteristics of earthquake-induced liquefaction features, *in* Crone, A.J., and Omdahl, E.M., editors, Directions in paleoseismology: Denver, Colorado, Proceedings of Conference XXXIX, U.S. Geological Survey Open-File Report 87-673, p. 173-177.

Obermeier, S.F., Jacobson, R.B., Smoot, J.P., Weems, R.E., Gohn, G.S., Monroe, J.E., and Powars, D.S., 1990, Earthquake-induced liquefaction features in the coastal setting of South Carolina and in the fluvial setting of the New Madrid seismic zone: U.S. Geological Survey Professional Paper 1504, 44 p.

Olig, S.S., Lund, W.R., Black, B.D., and Mayes, B.H., 1996, Paleoseismic investigation of the Oquirrh fault zone, Tooele County, Utah, *in* Lund, W.R., editor, Paleoseismology of Utah, Volume 6, The Oquirrh fault zone, Tooele County, Utah - Surficial geology and paleoseismicity: Utah Geological Survey Special Study 88, p. 22-64.

Oviatt, C.G., and Currey, D.R., 1987, Pre-Bonneville Quaternary lakes in the Bonneville basin, *in* Kopp, R.S., and Cohenour, R.E., editors, Cenozoic geology of western Utah - Sites for precious metal and hydrocarbon accumulations: Utah Geological Association Publication 16, p. 257-263.

Oviatt, C.G., Currey, D.R., and Miller, D.M., 1990, Age and paleoclimatic significance of the Stansbury shoreline of Lake Bonneville, northeastern Great Basin: Quaternary Research, v. 33, p. 291-305.

Oviatt, C.G., Currey, D.R., and Sack, Dorothy, 1992, Radiocarbon chronology of Lake Bonneville, eastern Great Basin, USA: Palaeogeography, Palaeoclimatology, Palaeoecology, v. 99, p. 225-241.

Personius, S.F., 1990, Surficial geologic map of the Brigham City segment and adjacent parts of the Weber and Collinston segments, Wasatch fault zone, Box Elder and Weber Counties, Utah: U.S. Geological Survey Miscellaneous Investigations Map I-1979, scale 1:50,000.

Peterson, D.L., and Oriel, S.S., 1970, Gravity anomalies in Cache Valley, Cache and Box Elder Counties, Utah, and Bannock and Franklin Counties, Idaho: U.S. Geological Survey Professional Paper 700-C, Geological Survey Research 1970, Chapter C, p. C114-C118.

Rhode, David, and Madsen, D.B., 1995, Late Wisconsin/early Holocene vegetation in the Bonneville Basin: Quaternary Research, v. 44, p. 246-256.

Schwartz, D.P., Lund, W.R., Mulvey, W.E., and Budding, K.E., 1988, New paleoseismicity data and implications for space-time clustering of large earthquakes on the Wasatch fault zone, Utah [abs.]: Seismological Research Letters, v. 59, no. 1, p. 15.

Scott, W.E., and Shroba, R.R., 1985, Surficial geologic map of an area along the Wasatch fault zone in the Salt Lake Valley, Utah: U.S. Geological Survey Open-File Report 85-448, 18 p., scale 1:24,000.

Seed, H.B., and Idriss, I.M., 1971, Simplified procedure for evaluating soil liquefaction potential: Proceedings of the American Society of Civil Engineers, Journal of the Soil Mechanics and Foundations Division, v. 97, no. SM9, p. 1249-1273.

Seed, H.B., Mari, K., and Chan, C.K., 1977, Influence of seismic history on liquefaction of sands: Proceedings of the American Society of Civil Engineers, Journal of the Geotechnical Engineering Division, v. 103, no. GT4, p. 257-270.

Shroba, R.R., 1980, Influence of parent material, climate, and time on soils formed in Bonneville-shoreline and younger deposits near Salt Lake City and Ogden, Utah [abs.]: Geological Society of America Abstracts with Programs, v. 12, no. 6, p. 304.

Smith, R. B., and Arabasz, W.J., 1991, Seismicity of the Intermountain seismic belt, *in* Slemmons, D.B., Engdahl, E.R., Zoback, M.D., and Blackwell, D.D., editors, Neotectonics of North America: Boulder, Colorado, Geological Society of America, Decade Map Volume 1, p. 185-228.

Smith, R.B., and Bruhn, R.L., 1984, Intraplate extensional tectonics of the eastern Basin-Range -Inferences on structural style from seismic reflection data, regional tectonics, and thermal-mechanical models of brittle-ductile deformation: Journal of Geophysical Research, v. 89, no. B7, p. 5733-5762.

Soil Survey Staff, 1981, Soil survey manual - Examination and description of soils in the field (Chapter 4): U.S. Department of Agriculture, unpublished Soil Conservation Service manuscript, p. 4-1 to 4-107.

Stuiver, M., and Reimer, P.J., 1993, Extended $^{14}C$ database and revised CALIB radiocarbon calibration program: Radiocarbon, v. 35, p. 215-230.

Tinsley, J.C., Youd, T.L., Perkins, D.M., and Chen, A.T.F., 1985, Evalu-

ating liquefaction potential, *in* Ziony, J.I., editor, Evaluating earthquake hazards in the Los Angeles region - An earth-science perspective: U.S. Geological Survey Professional Paper 1360, p. 263-315.

Van Horn, Richard, 1975, Largest known landslide of its type in the United States - A failure by lateral spreading in Davis County, Utah: Utah Geology, v. 2, no. 1, p. 83-87.

Viveiros, J.J., 1986, Cenozoic tectonics of the Great Salt Lake from seismic reflection data: Salt Lake City, University of Utah, M.S. thesis, 81 p.

Wieczorek, G.F., Wilson, R.C., and Harp, E.L., 1985, Map showing slope stability during earthquakes in San Mateo County, California: U.S. Geological Survey Miscellaneous Geologic Investigations Map I-1257E, scale 1:62,500.

Wilson, R.C., and Keefer, D.K., 1985, Predicting areal limits of earthquake-induced landsliding, *in* Ziony, J.I., editor, Evaluating earthquake hazards in the Los Angeles region - An earth- science perspective: U.S. Geological Survey Professional Paper 1360, p. 316-345.

Youd, T.L., 1977, Discussion of "Brief review of liquefaction during earthquakes in Japan," by E. Kuribayashi and F. Tatsuoka: Soils and Foundations, v. 17, no. 1, p. 82-85.

— 1978, Major cause of earthquake damage is ground failure: Civil Engineering, American Society of Civil Engineers, v. 48, no. 4, p. 47-51.

— 1980, Ground failure displacement and earthquake damage to buildings: Knoxville, Tennessee, American Society of Civil Engineers, Proceedings, Conference on Civil Engineering and Nuclear Power, v. 2, p. 7-6-1 - 7-6-26.

— 1984, Geologic effects - Liquefaction and associated ground failure, *in* Kitzmiller, Carla, compiler, Proceedings of the geologic and hydrologic hazards training program: U.S. Geological Survey Open-File Report 84-760, p. 210-232.

Youd, T.L., and Perkins, D.M., 1987, Mapping of liquefaction severity index: Journal of Geotechnical Engineering, v. 113, no. 11, p. 1374-1392.

Youngs, R.R., Swan, F.H., Power, M.S., Schwartz, D.P., and Green, R.K., 1987, Probabilistic analysis of earthquake ground shaking hazard along the Wasatch Front, Utah, *in* Gori, P.L., and Hays, W.W., editors, Assessment of regional earthquake hazards and risk along the Wasatch Front, Utah, Volume II: U.S. Geological Survey Open-File Report 87-585, p. M1-M110.

Zoback, M.L., 1983, Structure and Cenozoic tectonism along the Wasatch fault zone, Utah, *in* Miller, D.M., Todd, V.R., and Howard, K.A., editors, Tectonic and stratigraphic studies in the eastern Great Basin: Geological Society of America Memoir 157, p. 3-28.

— 1992, Superimposed late Cenozoic, Mesozoic, and possible Proterozoic deformation along the Wasatch fault zone in central Utah, *in* Gori, P.L., and Hays, W.W., editors, Assessment of regional earthquake hazards and risk along the Wasatch Front, Utah: U.S. Geological Survey Professional Paper 1500-A-J, p. E1-E20.

# APPENDIX A

## DESCRIPTIONS OF TRENCH UNITS

### Trench FST1

**Landslide deposits derived from lacustrine sediment:**

**Unit 1** Interbedded fine sand, silty fine sand, and clayey silt with very fine sand. Fine sand is olive brown (2.5Y 4/3[1]); micaceous; very well sorted; structureless to poorly bedded with brown (10YR 5/3) silty fine sand; bed thickness 2-11 cm. Clayey silt is brown (10YR 5/3) to olive brown (2.5Y 4/3); moderately plastic[2]; 5% very fine sand, 95% fines[3]; bed thickness 0.5-2 cm. Unit has no visible $CaCO_3$; no to slight reaction with HCl; uncemented; gently folded with small brittle offsets (microfaults) evident in clay layers; lower contact not exposed; upper contact conformable/gradational with unit 2; locally juxtaposed against units 2 and 3 along shear surface.

**Unit 2** Interbedded fine sand and clayey silt with very fine sand. Fine sand is yellowish brown (10YR 5/4); very well sorted; structureless; bed thickness 14-18 cm. Clayey silt is brown (10YR 5/3); moderately plastic; laminated; 1% very fine sand, 99% fines; bed thickness 2-3 cm. Unit has no visible $CaCO_3$; no to slight reaction with HCl; uncemented; gently folded with small brittle offsets (microfaults) evident in clay layers; lower and upper contacts conformable/gradational with units 1 and 3; locally juxtaposed against units 1 and 3 along shear surfaces; locally grades upward into unit S1(Bk).

**Unit 3** Interbedded clayey silt and fine sand with silt. Clayey silt is brown (10YR 5/3); moderately plastic; laminated with a distinctive green horizon; moderate oxidation along partings; bed thickness 10-24 cm. Fine sand is yellowish brown (10YR 6/4); well sorted; structureless to thin bedded with green and brown silt horizons; 95% sand, 5% fines; bedding thickness 6-10 cm. Unit has no visible $CaCO_3$; slight reaction with HCl in silt, no reaction in sand; uncemented; gently folded; lower contact conformable/gradational with unit 2; locally juxtaposed against units 1 and 2 along shear surfaces; grades upward into unit S1(Bk).

**Modern soil:**

**Unit S1(Bk)** Bk horizon developed in units 2 and 3; clayey silt with very fine sand; dark yellowish brown (10YR 4/4); moderately plastic; few soft $CaCO_3$ nodules at base of unit, scattered filaments throughout (stage I+ carbonate morphology[4]); vigorous reaction with HCl; uncemented; diffuse lower boundary; clear upper boundary.

**Unit S1(A)** A horizon; clayey silt with fine sand; dark grayish brown (10YR 4/2); granular structure; moderately plastic; abundant rootlets; no visible $CaCO_3$; vigorous reaction with HCl; uncemented; clear lower boundary.

### Trench FST2

**Disturbed lacustrine sediments:**

Unit 1 Fine sand with a trace of silt; brown (10YR 5/3); well sorted; structureless with thin (1-4 cm), poorly laminated, disrupted silt beds; 95% sand, 5% fines; scattered Fe-oxide mottling; no visible $CaCO_3$ or reaction with HCl; uncemented; scattered, minor bioturbation; lower contact not exposed; upper contact conformable/sharp with unit 2; locally overlain by units S1(Bkb) and S2(Bk).

Unit 2 Clayey silt with fine sand; brown (7.5YR 5/3); poorly laminated; slightly plastic; 5% sand, 95% fines; no visible $CaCO_3$; moderate reaction with HCl; uncemented; scattered, minor bioturbation; locally cross-cut by sand dikes (1-4 cm thick) from unit 1; lower contact conformable/sharp with unit 1; grades upward into units S1(Bkb) and S2(Bk).

**Paleosol:**

Unit S1(Bk) Bk horizon developed in unit 2; clayey silt with fine sand; yellowish brown (10YR 5/4);

---

[1]*Munsell colors reported are for moist material unless otherwise noted.*

[2]*Plasticity estimated in the field; for coarse-grained units plasticity is reported for the matrix (fine portion) of the deposit.*

[3]*Reported percentages of grain-size fractions are field estimates using the American Society for Testing and Materials (ASTM) D 2488-90 (Visual-Manual Procedure) classification system.*

[4]*Carbonate morphology from Gile and others (1966), Machette (1985), and Birkeland and others (1991).*

slightly plastic; few soft and locally abundant hard $CaCO_3$ nodules, pervasive filaments throughout (stage II carbonate morphology); vigorous reaction with HCl; weakly cemented; extensive bioturbation; abrupt to gradual lower boundary; clear to diffuse upper boundary.

**Unit S1(Bkb)** Same as unit S1(Bk), but buried by unit 3.

**Colluvial wedge:**

**Unit 3** Colluvial soil derived from eroded scarp free face; silty fine sand with clay, gravel, and disseminated organic matter; dark grayish brown (10YR 4/2); moderately sorted; structureless; pervasive pinhole texture (vesicular); moderately plastic; 5% gravel[5], 60% sand, 35% fines; maximum clast size 2 cm; subangular to subround; sand is micaceous; pervasive $CaCO_3$ filaments (stage I carbonate morphology); vigorous reaction with HCl; uncemented; wedge-shaped unit with indistinct upper and lower contacts; pinches out towards the east; western end juxtaposed against units 2 and S1(Bk) along sharp, steep, east-dipping contact (buried scarp free face).

**Modern soil:**

**Unit S2(Bk)** Bk horizon developed in units 2 and 3; locally overprints unit S1(Bk); sandy silt with clay and gravel; brown to dark brown (10YR 4/3); moderately plastic; 5% gravel, 25% fine sand, 70% fines; maximum clast size 2 cm; scattered fine rootlets; scattered to pervasive $CaCO_3$ filaments (stage I to stage II carbonate morphology); moderate to vigorous reaction with HCl; uncemented; locally extensive bioturbation; gradual lower boundary; clear upper boundary.

**Unit S2(A)** A horizon; clayey silt with gravel and fine sand; very dark grayish brown (10YR 3/2); granular structure; slightly plastic; abundant rootlets; no visible $CaCO_3$; moderate reaction with HCl; uncemented; clear lower boundary.

## Trench FST3

**Landslide deposits derived from lacustrine sediment:**

**Unit 1** Cyclically bedded fine sand and clayey silt. Fine sand is olive brown (2.5Y 4/4) and yellowish brown (10YR 5/4); well sorted; stratified; bed thickness 1-4 cm. Clayey silt is yellowish brown (10YR 5/4); moderately plastic; laminated to thin bedded (up to 3 cm thick). Unit contains thin (1-3 cm), disrupted lens of coarse sand and gravel at north end of trench (possible channel deposit); no visible $CaCO_3$ at north end of trench, but abundant, hard nodules in clay horizons at south end of trench; slight to moderate reaction with HCl; uncemented; deformation characterized by inclined bedding offset by high-angle faults; clay beds locally cross-cut by sand dikes; lower contact not exposed; upper contact conformable/gradational with unit 2; locally juxtaposed against unit 2 along shear surfaces; locally grades upward into unit S2(Bk2).

**Unit 2** Clayey silt with minor interbedded fine sand. Clayey silt is yellowish brown (10YR 5/4) to light brownish gray (2.5Y 6/2) with some olive (5Y 5/6) horizons; moderately plastic; laminated to thin bedded (up to 3 cm thick). Fine sand is yellowish brown (10YR 5/4) to olive gray (5Y 4/2); very well sorted; structureless; bed thickness 0.5-12 cm. Unit has sparse Fe-oxide mottling; no visible $CaCO_3$; slight reaction with HCl; uncemented; gently to strongly folded with local convolute lamination; clay beds locally cross-cut by sand dikes (1-7 cm thick); lower contact conformable/gradational with unit 1; locally juxtaposed against units 1, 3, and S1(A) along shear surfaces and unconformities; locally grades upward into unit S2(Bk2).

**Unit 3** Clayey silt; pale yellow (2.5Y 7/3) to pale brown (10YR 6/3); slightly plastic; structureless to brecciated; pervasive pinhole texture (vesicular); sparse Fe-oxide mottling; sparse $CaCO_3$ filaments and pore infillings (stage I carbonate morphology); moderate reaction with HCl; uncemented; scattered distribution, locally juxtaposed unconformably and along shear surfaces against unit 2; contains abundant dark soil blocks (paleosols and/or infilled burrows); locally grades upward into unit S2(Bk2).

**Paleosol:**

**Unit S1(A)** A horizon soil blocks incorporated into landslide deposits; silt with clay and fine sand; color blotchy, but averages very dark grayish brown (10YR 3/2); slightly plastic; structureless; pervasive pinhole texture (vesicular); sand is micaceous; no visible $CaCO_3$; moderate reaction with HCl; uncemented; sharp contacts with units 2 and 3; locally overprinted by units S2(Bk2) and S2(Bk1).

[5]*Clast composition is predominantly metamorphic (gneiss, amphibolite) unless otherwise noted.*

**Modern soil:**

**Unit S2(Bk2)** Bk horizon developed in units 1, 2, 3, and S1(A); silt and clayey silt with varying amounts of sand depending on parent material; average color very pale brown (10YR 7/3); slightly to moderately plastic; abundant $CaCO_3$ filaments, soil matrix whitened by $CaCO_3$, locally abundant nodules (stage II carbonate morphology); vigorous reaction with HCl; weakly cemented; moderate bioturbation; gradual lower boundary; clear to gradual upper boundary.

**Unit S2(Bk1)** Bk horizon overlying unit S2(Bk2); silt and clayey silt with sand; brown (10YR 4/3); moderately plastic; scattered fine rootlets; abundant $CaCO_3$ filaments (stage I carbonate morphology); vigorous reaction with HCl; uncemented; moderate bioturbation; gradual lower boundary; clear to gradual upper boundary; grades laterally into units S2(Bt) and S2(Bw).

**Unit S2(Bt)** Weakly developed Bt horizon; clay; pale brown (10YR 6/3); weakly developed angular blocky structure; plastic; abundant rootlets; no visible $CaCO_3$; no to slight reaction with HCl; uncemented; gradual lower and upper boundaries; grades laterally into unit S2(Bk1).

**Unit S2(Bw)** Weakly developed Bw horizon; clayey silt with fine sand; yellowish brown (10YR 5/4) to dark yellowish brown (10YR 4/6); slightly plastic; abundant fine rootlets; scattered $CaCO_3$ filaments (stage I carbonate morphology); vigorous reaction with HCl; uncemented; gradual lower boundary; clear upper boundary; grades laterally into unit S2(Bk1).

**Unit S2(A)** A horizon; clayey silt with fine sand; very dark gray (10YR 3/1); granular structure; slightly plastic; abundant rootlets; no visible $CaCO_3$; no to slight reaction with HCl; uncemented; clear to gradual lower boundary.

## Trench FST4

**Landslide deposits derived from lacustrine sediment:**

**Unit 1** Sandy silt and clay with scattered fine gravel; yellowish brown (10YR 5/6); moderately plastic; laminated to bedded with thin (0.2-2 cm) sand horizons; 5% gravel, 40% sand, 55% fines; maximum clast size 10 cm; gravel subangular/tabular to subround; no visible $CaCO_3$; slight reaction with HCl; uncemented; strongly folded (recumbent, isoclinal folds and convolute lamination); lower contact not exposed; locally juxtaposed against units 2 and 3 along shear surfaces; locally grades upward into unit S1(Bk).

**Unit 2** Interbedded clay, silt, and clayey very fine sand. Clay is yellowish brown (10YR 5/4); moderately plastic. Silt is yellowish brown (10YR 5/4); non-plastic; interlaminated with clay. Sand is olive brown (2.5Y 4/3); micaceous; well sorted; moderately plastic. Unit has no visible $CaCO_3$; no reaction with HCl in sand, slight reaction in clay; uncemented; 30% sand, 70% fines; bed thickness 1-3 cm; gently folded and locally faulted; juxtaposed against unit 1 along shear surface (fault marked by thin layer of fine to medium sand and fine gravel); grades upward into unit S1(Bk).

**Unit 3** Clayey silt with sand and scattered gravel; yellowish brown (10YR 5/4); moderately plastic; blocky structure; laminae locally preserved within blocks; scattered lenses and stringers of olive (5Y 4/4), well-sorted fine sand; 10% gravel, 10% sand, 80% fines; dominant gravel clast size 1-2 cm, maximum clast size 6 cm; angular to round; no visible $CaCO_3$; moderate reaction with HCl; uncemented; unit is enclosed within unit 1 with sharp to obscure, unconformable (fault?) contact; grades upward into unit S1(Bk).

**Modern soil:**

**Unit S1(Bk)** Bk horizon developed in units 1, 2, and 3; clayey silt with scattered sand and gravel; light yellowish brown (10YR 6/4); plastic; 10% gravel, 10% sand, 80% fines; maximum clast size 3 cm; scattered fine rootlets; scattered $CaCO_3$ filaments and pore fillings (stage I carbonate morphology); moderate to vigorous reaction with HCl; uncemented; local bioturbation; diffuse lower boundary; gradual upper boundary.

**Unit S1(Bw)** Weakly developed Bw horizon; clayey silt; yellowish brown (10YR 5/4); homogeneous texture; moderately plastic; sparse fine rootlets; no visible $CaCO_3$; vigorous reaction with HCl; uncemented; local bioturbation; gradual lower boundary; clear upper boundary.

**Unit S1(A)** A horizon; clayey silt with gravel; very dark grayish brown (10YR 3/2); granular structure; moderately plastic; abundant rootlets; no visible $CaCO_3$; moderate to vigorous reaction with HCl; uncemented; clear lower boundary.

## Trench FST5 (Composite)

**Older landslide deposits derived from lacustrine sediment:**

**Unit 1** Silty fine sand with a trace of clay, and fine sand with silt. Silty sand is gray (10YR 5/1); micaceous; moderately plastic; structureless; 75% sand, 25% fines; sparse Fe-oxide mottling. Sand with silt is very dark grayish brown (10YR 3/2); micaceous; non-plastic; structureless; 90% sand, 10% fines. Unit has no visible $CaCO_3$; no reaction with HCl; uncemented; sand with silt occurs as pockets within the silty sand; lower contact not exposed; grades upward into unit S1(Bt2) in test pits B, C, and D; upper contact unconformable/sharp with unit 2 in test pit E.

**Unit 2** Clay with fine sand and a trace of silt, and silty fine sand. Clay is brown (10YR 5/3) to very dark gray (10YR 3/1); micaceous; plastic; thin, discontinuous, inclined bedding; bed thickness 3-6 cm; 5% sand, 95% fines. Silty sand is gray (10YR 5/1); micaceous; non-plastic; structureless; 80% sand, 20% fines; pervasive Fe-oxide mottling; forms prominent lens. Unit has no visible $CaCO_3$; no reaction with HCl; uncemented; lower contact unconformable/sharp with unit 1; grades upward into Unit S1(Bt2).

**Paleosol:**

**Unit S1(Bt2)** Weak Bt horizon developed in units 1 and 2; clay with fine sand and disseminated organic matter; very dark grayish brown (10YR 3/2); plastic; scattered fine rootlets; no visible $CaCO_3$; no reaction with HCl; uncemented; gradual lower boundary; clear upper boundary.

**Unit S1(Bt1)** Weakly developed Bt horizon overlying unit S1(Bt2); similar to unit S1(Bt2), but slightly gleyed; dark grayish brown (10YR 4/2); gradual upper boundary except where locally overlain by unit 3 with sharp contact.

**Unit S1(A)** A horizon; clay with fine sand; black (10YR 2/1); micaceous; weakly developed granular structure; plastic; abundant rootlets; no visible $CaCO_3$; no reaction with HCl; uncemented; gradual lower boundary; diffuse upper boundary except where locally overlain by unit 3 with unconformable/sharp contact.

**Younger landslide deposit derived from lacustrine sediment:**

**Unit 3** Silty fine sand with scattered pockets and discontinuous beds of fine to medium sand with a trace of silt; grayish brown (10YR 5/2) to dark grayish brown (10YR 4/2); moderately to very well sorted; micaceous; slightly plastic; unstratified in test pit A, poorly developed horizontal bedding in test pit B; bed thickness 1-4 cm; contains numerous, variously oriented fragments of dark, organic-rich material (possible infilled burrows); 80-98% sand, 2-20% fines; pervasive Fe-oxide mottling; no visible $CaCO_3$; no reaction with HCl; uncemented; wedge-shaped unit, pinches out towards the east (as exposed in test pit B); lower contact unconformable/sharp with units S1(Bt1) and S1(A); generally grades upward into unit S2(A), but locally overlain by unit S2(Ap) with sharp contact.

**Modern soil:**

**Unit S2(A)** A horizon; clayey silt with fine sand; very dark brown (10YR 2/2); weakly developed granular structure; moderately plastic; scattered rootlets; pervasive Fe-oxide staining (strong brown; 7.5YR 4/6); no visible $CaCO_3$; no reaction with HCl; uncemented; gradual lower boundary; diffuse upper boundary.

**Unit S2(Ap)** Cultivated A horizon; clayey silt; black (10YR 2/1); granular structure; slightly plastic; abundant rootlets; no visible $CaCO_3$; no reaction with HCl; uncemented; diffuse to clear lower boundary.

# APPENDIX B

## RADIOCARBON ANALYSES AND CALIBRATIONS

Radiocarbon dating of bulk-sediment samples from the trenches provided limiting estimates of landslide timing. We obtained low-carbon-content samples ranging in size from approximately 1 to 2.5 kilograms (2-5 lb) from the base of soil A horizons and middle of paleosol blocks incorporated into the landslide deposits. We did not apply carbon mean-residence-time (MRT) corrections because the ages of samples obtained from the base of A horizons are believed to approximate the time when the soil began forming, and because of uncertainty in applying an appropriate correction to ages of samples obtained from the paleosol blocks.

The samples were analyzed by Beta Analytic, Inc. of Miami, Florida, the same laboratory that analyzed samples obtained from the Farmington Siding landslide complex by Harty and others (1993). All of the samples were analyzed by conventional radiometric techniques except FST5b-RC2 (Beta-81830), which was analyzed by accelerator mass spectrometry (AMS). Sample pretreatment consisted of acid (HCl) washes for conventional analysis, and acid and alkali (NaOH) washes for AMS analysis. All of the radiocarbon ages were $\delta^{13}C$ corrected.

We converted radiocarbon ages to calendric ages (0 yr BP = AD 1950) using the methods of Stuiver and Reimer (1993). We used a bidecadal calibration data set, assigned a laboratory error multiplier of 2 to each age estimate, and smoothed the calibration curve using a 100-year moving average. The calibrated ages were rounded to the nearest 50 years and are reported with $2\sigma$ intercepts.